國 立 清 華 大 學
材料科學工程研究所
碩士論文

以化學方法合成鐵鉑合金奈米微粒與磁性質之研究

Study on the synthesis of FePt nanoparticles and magnetic properties

指導教授： 賴志煌 教授 **(Prof. Chih-Huang Lai)**

研 究 生： 鍾加琪 **(Chia-Chi Chung)**

學　　號： **9631513**

中 華 民 國 九 十 八 年 六 月

摘要

磁性奈米微粒近年來受到廣大的關注，在生醫方面，例如:藥物投遞(drug delivery)、核磁共振造影(MRI)，或是在記錄媒體上，廣泛被應用。其中在記錄媒體方面，鐵鉑合金(FePt)最受矚目，因其具有高異向性，可解決超順磁所產生的問題。所謂超順磁現象，意旨當粒子尺寸趨近奈米尺寸時，磁矩易受到熱擾動的影響。

鐵鉑奈米微粒的合成目前遇到最大瓶頸在於，其尺寸不易增大。再者，當尺寸增大時，鐵和鉑的比例會受到尺寸的影響而形成鉑偏多的鐵鉑微粒。然而，鐵鉑合金的磁性質易受到成分的影響，當鐵和鉑的比例偏離一比一時，矯頑場(H_c)會有很明顯的下降。

論文主軸是以化學方法合成鐵鉑合金奈米微粒，藉由調變合成參數，例如:界面活性劑、加熱時間以及加熱溫度，來改變微粒尺寸以及成分。並探討這些合成參數對尺寸和成分的影響。再藉由後退火處理，使鐵鉑合金產生序化。我們採用鐵鉑合金微粒和食鹽混合來防止奈米微粒在高溫熱處理下產生聚集。從實驗結果可知，食鹽可作為阻絕層，有效防止奈米微粒在高溫下的聚集。最後，將探討 FePt 和 $FePt_3$ 之間的交互耦合作用在磁性質上的特殊性。

Abstract

The larger size of FePt nanoparticles is a big challenge in recent years. In my work, controlling size distribution and composition of FePt nanoparticles by thermodecomposition method is the main topic. As-synthesized FePt nanoparticles are chemically disordered and post-annealing is required to obtain chemically ordered FePt. Salt matrix-aid effect in annealing steps of as-synthesized FePt nanoparticles and the magnetic properties of annealed FePt alloy are studied. The exchange coupling phenomenon between FePt (FM) and $FePt_3$ (AFM) nanoparticles was demonstrated and discussed in the final section.

Contents

List of Figures

List of tables

Chapter 1 Introduction

Magnetic nanoparticles have drawn much attention in recent years due to their possible applications on the data storage, magnetic fluids, catalysis, biomedicine, and magnetic resonance imaging. They possess unique properties due to their quantum size effects and large surface area.

Spherical nanoparticles can occupy only 70% of the area in a two dimensional array, so the packing fraction is very low. Increasing the packing fraction and obtaining alignment of the magnetic axis are both crucial for utilization of chemically synthesized magnetic nanoparticles. Control of nanoparticles shape opens the door to their being used in various technological applications that spherical nanoparticles cannot achieve.

1.1 Motivation

FePt nanoparticles have been intensively studied in recent years because of their unique magnetic properties. There are three major different types of ordered FePt alloys, namely, Fe_3Pt, FePt, $FePt_3$. The fct-structured FePt nanoparticles are particularly desirable because of its high magnetic anisotropy, high coercivity, and chemical stability. On the other hand, FePt nanoparticles, a material widely used in data storage and permanent magnetic nanocomposite, also possess a great potential in biomedicine.

However, the synthesis of larger FePt nanoparticles (>6nm) with a

near-equal atomic percentage is still a big challenge. The ideal FePt nanoparticle size is 3-15 nm. In my work, the effect of some synthetic parameters, including the surfactant concentration, the heating time, and the heating temperature, is discussed. $L1_0$ FePt and $FePt_3$ possess different magnetic properties. So the interaction between FePt and $FePt_3$ is an interesting issue.

Chapter 2 Background

2.1 Special Features of Magnetic Nanoparticles

2.1.1 Superparamagnetism

Nanoparticles that are made of a ferro- of ferrimagnetic material, and below a certain size as well as higher than blocking temperature, can exhibit a unique form of magnetism called superparamagnetism. This important phenomena present only in nanoparticle systems.

Magnetism is highly volume and temperature dependent because this property arises from the collective interaction of atomic magnetic dipoles. When the size of a ferro- or ferrimagnet decrease to a certain critical value r_c, the particles change from a state with multiple magnetic domains to one with a single domain.

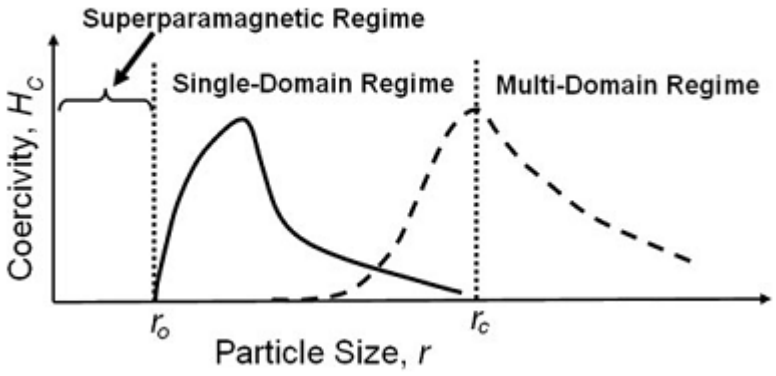

Figure 2.1 *The dependence of magnetic coercivity on particle size[1]*

As shown in Figure2.1 [1], if the size continues to decrease to a value r_0 ,the thermal energy becomes comparable with that required for spin to flip direction, leading to the randomization of the magnetic dipoles in a short period of time. Such small particles do not have permanent magnetic moments in the absence of an external field.

There are two characteristics in superparamagnetism:

(1) Superparamagnetism is regarded as an assembly of giant magnet, and they are not interacting. They can fluctuate when thermal energy, K_BT, is larger than the anisotropy energy.

(2) Superparamagnetic nanoparticles exhibit no remanence or coercivity, that is, there is no hysteresis in the M-H curve.

The magnetization trends of supermagnetic nanoparticles are similar to paramagnetic nanoparticles. They both have no coercivity in the absence of the applied field. However, the reasons for the lack of remanence are different. In paramagnetic nanoparticles, the induced moment is in the same direction as the applied field, and grows with increasing magnetic field until reaching saturation. Paramagnetic nanoparticles do not have strong interaction with neighbors. So there is very little activation energy to be overcome in these processes, and therefore paramagnetic nanoparticles do not exhibit hysteresis. However, because the superparamagnetism is a balance between magnetic energy and thermal energy, the phenomenon occurs only in the limited range of size and temperature. In the superparamagnetic system, at zero field the net magnetization of a large ensemble of superparamagnetic particles is zero, but the magnetization of each individual particle remains at its fixed

value. The zero magnetization in the absence of the applied field is due to the random orientation of the various particles' spins.

Understanding and controlling the superparamagnetic properties of nanoparticles is vital to many important applications. The superpara-magnetism of magnetic nanoparticles become the fundamental density limit for magnetic memory device. Interesting, these superpara- magnetic nanoparticles are very useful for biomedical application, because they are not subject to magnetic interactions in a dispersion and are stable in physiological condition [2].

2.1.2 Single domain

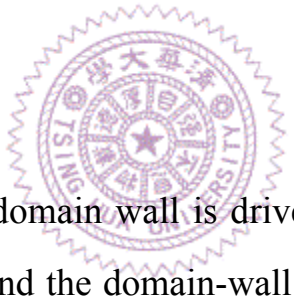

The formation of the domain wall is driven by the balance between the magnetostatic energy and the domain-wall energy. The magnetostatic energy increases proportionally to the volume of the materials and the domain wall energy increases proportionally to the interfacial area between domains. When the magnetic nanoparticle size is reduced to the critical volume, it costs more energy to create a domain wall than to support the magnetostatic energy. Therefore, these nanoparticles exhibit single-domain states. The critical diameter typically lies in the range of a few tens of nanometers and depends on the material.

The critical diameter of a spherical particle, D_c, is reached when the magnetostatic energy is equal to the domain-wall energy. D_c can be expressed as [3]

$$D_c = \frac{1.7\,\gamma}{\pi^2 M_S^2}$$

Where γ is domain-wall energy and M_s is saturation magnetization. According to the above equation, the domain walls hardly exist in the nanoparticles when the domain-wall energy grows. So the nanoparticles are the single-domain states.

Typical values of D_c for some magnetic materials are listed in Table 2.1 [4].

Table 2.1 *Single-domain size for different spherical particles[4]*

Material	D_c [nm]
hcp Co	15
fcc Co	7
Fe	15
Ni	55
$SmCo_5$	750
Fe_3O_4	128

A single-domain particle is uniformly magnetized with all the spins aligned in the same direction. The magnetization will be reversed by spin rotation since there are no domain walls to move. This is the reason for the very high coercivity observed in small nanoparticles.

2.1.3 Surface Anisotropy

As the physical dimension of magnetic nanoparticles decreases, the ratio of surface to volume increases, resulting in the surface properties significant. Owing to the larger surface-to-volume ratio, the surface spins

make an important contribution to the magnetization. Surface anisotropy in ultrathin metallic films may cause an orientation of magnetization perpendicular to the surface of the film and leads to out-of-plane anisotropy which is useful for perpendicular magnetic recording. However, in magnetic nanoparticles, the surface anisotropy leads to the moment unstable. The surface anisotropy originates from broken symmetry at the surface, surface-core strains, and magnetostriction. If influences the spin configuration of the nanoparticle core via exchange coupling. From Figure 2.2, when the surface anisotropy(K_s) is larger than magnetocrystalline anisotropy(K_v), the spin of outer shell tend to orient normal to the surface [5].

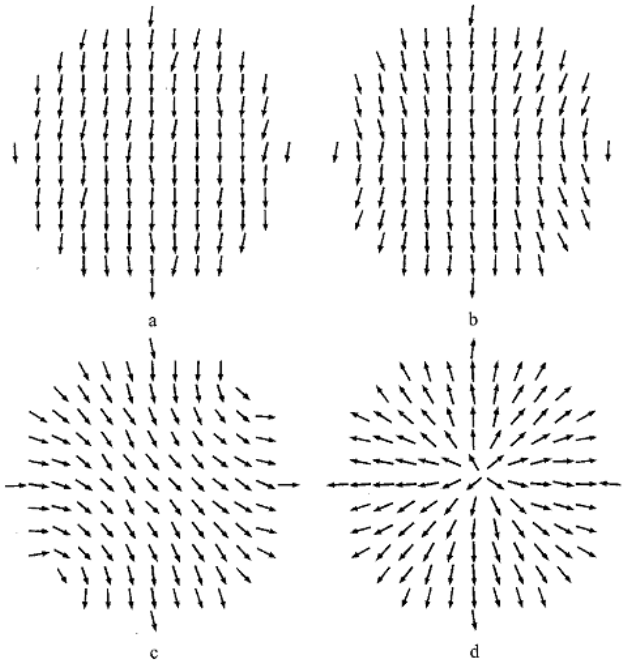

Figure 2.2 *The difference of K_s and K_v leads to the variation of spin structure within the nanoparticles. K_s / K_v =(a) 1, (b)10, (c) 40, and (d) 60[5]*

Bødker et al. reported that the magnetic anisotropy constant of iron nanoparticles increases with decreasing particle size, due to the influence of surface anisotropy. They showed the total energy barrier written as:

$$\triangle E_a = K'_{eff} V = K'_V V + K'_s S$$

Where K'_V and K'_s are the volume and the surface anisotropy energy constants, respectively, S is the surface area, and V is the volume. Assuming that the particles are spherical with diameter *d*, the equation can be written as [6]

$$K'_{eff} = K'_V + \frac{6}{d} K'_s$$

Form the above equation, it was found that the value of K'_{eff} increases with decreasing particle size. We should notice that if the particles are assumed to have perfect spherical shape, this symmetry shows the total contribution of $\triangle E_a$ from surface anisotropy is zero. However, the nano-particles synthesized by chemical method are not perfectly spherical, so the net contribution from the surface effects is a result of deviations from spherical symmetry.

2.2 Introduction to Core/Shell Magnetic Nanoparticles

Magnetic core/shell nanoparticles can be categorized as those with magnetic core coated with a layer of a nonmagnetic, antiferromagnetic, or ferro/ferri-magnetic shell. A nonmagnetic coating is usually used for magnetic core stabilization, and surface functionalization for biomedical applications, such as Fe_3O_4/TiO_2 [8]. An antiferromagnetic coating over a ferromagnetic core leads to exchange bias and improvements in the thermal stability of the core.

2.2.1 Synthetic approaches to the core/shell nanoparticles

Synthetic methods were mainly divided into two categories. One is two steps processes, and the other is one-pot solvothermal synthesis. The followings are the concepts of the two methods.

The first bimagnetic core/shell nanoparticle was synthesized by Sun's group [7]. They are prepared by coating the existing FePt nanoparticles with Fe_3O_4 shell. For example, the 4-nm $Fe_{58}Pt_{42}$ nanoparticles are made by the combination of reduction of $Pt(acac)_2$ and decomposition of $Fe(CO)_5$ in the octyl ether solvent. The 4-nm FePt nanoparticles are then used as seeds and mixed with $Fe(acac)_3$ and 1,2-hexadenaediol, oleic acid, and oleylamine in phenyl ether solvent. Fe_3O_4 coating is achieved by heating the mixture. By controlling the material ratio of $Fe(acac)_3$ to FePt nanoparticle seeds, the Fe_3O_4 shell thickness can be tuned. Figure 2.3 shows a array of core/shell FePt/ Fe_3O_4 nanoparticles.

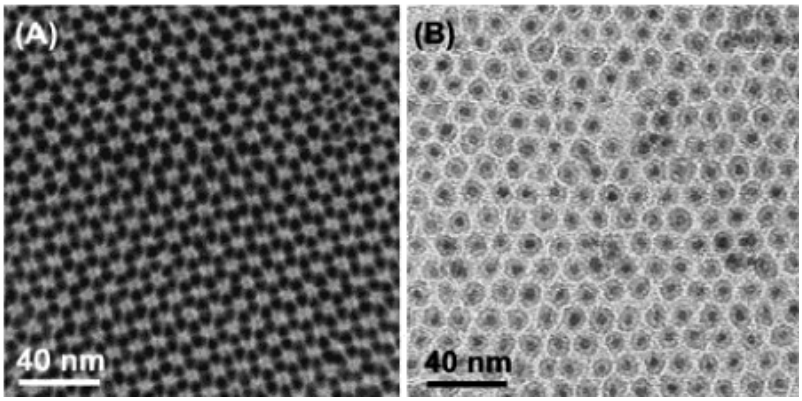

Figure 2.3 *TEM images of core/shell FePt/Fe_3O_4 nanoparticles with core/shell being (A) 4nm/0.5nm and (B) 4nm/2nm[7]*

Two-steps process can be applied on the synthesis of core/shell nanoparticles with a magnetic core and a metallic shell , such as Fe_3O_4/ Au[8], have also be demonstrated in recent years. The synthesis starts with Au nanoparticles by reducing $HAuCl_4$ in a chloroform solution of oleyl amine and coating Fe_3O_4 on the surfaces of Au nanoparticles. Figure 2.4 shows the process of the synthesis. The way they control the shell thickness is different from the above approach. The core/shell Fe_3O_4/ Au nanoparticles serves as seeds for the formation of Fe_3O_4/ Au nanoparticles with thicker Au by adding $HAuCl_4$ in the reducing condition.

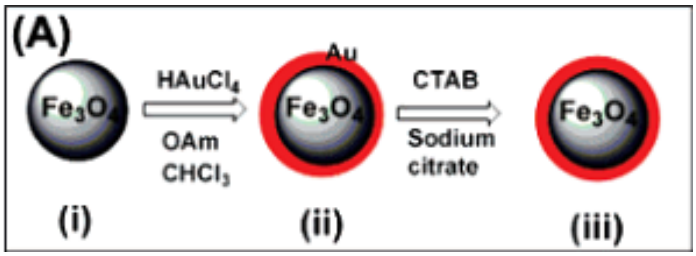

Figure 2.4 *Schematic illustration of surface coating of Fe_3O_4 nanoparticle with Au*

The other synthetic approach is one-pot solvethermal synthesis, in which all the reagents are present in the beginning [9-11]. The strategy is that the core material is prepared first, and then uses them as nucleation seeds to deposit the other components as the shell. The advantage of this method is very convenient since both homogeneous and heterogeneous nucleation processes of different materials can be controlled at once. Bimagnetic FePt/iron oxide nanoparticles were also demonstrated using the one-pot method. The mechanism involves homogeneous nucleation of FePt seeds and the subsequent heterogeneous growth of Fe_3O_4.

2.2.2 Magnetic properties of the core/shell nanoparticles

Core/shell structured nanoparticles, like ferromagnetic/ antiferro-magtic, nonmetallic/magnetic, and magnetic/magnetic, have particular magnetic properties due to the interaction between the interfaces. The exchange bias was observed in the nanoparticles consisting of a ferromagnetic Co core and an antiferromagnetic CoO shell when cooling down through the Néel temperature of the antiferromagnet. The main phenomenon of the exchange bias is a horizontal shift of the magnetic hysteresis loop after field cooling. The hysteresis loop shift accompanies with an increase of the coercivity, and can improve the performance of permanent magnetic materials. A recent review of exchange bias in nanostructured system is given by Nogués et al. [12].

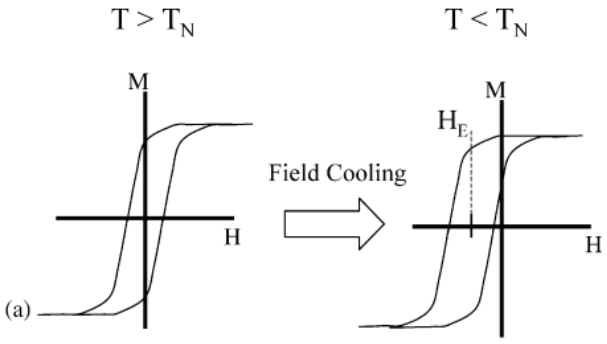

Figure 2.5 *Exchange bias causes the shift of the hysteresis loops[12]*

For core/shell Au/Fe_3O_4 nanoparticles, the saturation field increases from 1kOe for pure Fe_3O_4 nanoparticles to 10kOe for core/shell Au/Fe_3O_4 nanoparticles. The coercivity also increases from 200Oe to 800Oe. The remanence ratio(*S*) for pure Fe_3O_4 is about 0.8, which means a randomly oriented nanoparticle assembly with cubic anisotropy. However, for the core/shell Au/Fe_3O_4 nanoparticles, the *S* decreases to 0.5, which means a randomly oriented array with a uniaxial anisotropy. The hysteresis loops of 10nm Fe_3O_4 and 10nm Au/Fe_3O_4 nanoparticles with a 3nm Au core were shown in figure 2.6. The author explained that a new surface anisotropy was induced. Fe atoms at the Au/Fe_3O_4 interface have low nearest neighbors, which decreases the interatomic exchange coupling. Hence, the spins at the interface canted and they became hard to saturate [13].

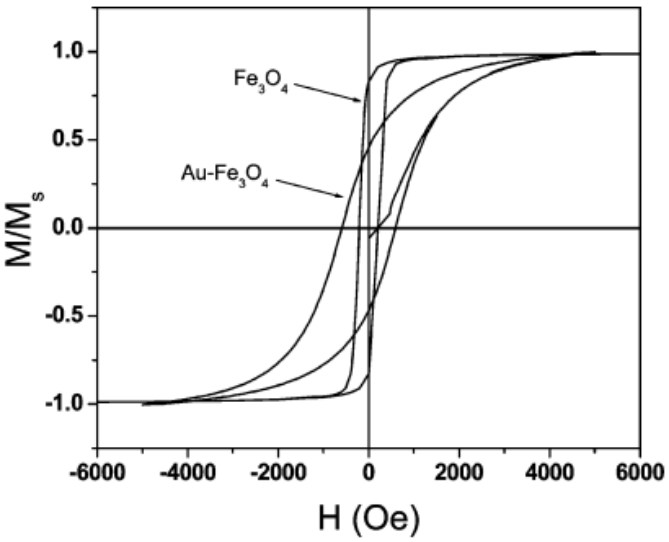

Figure 2.6 *The hysteresis loops of 10nm Fe_3O_4 nanoparticles and core/shell Au/Fe_3O_4 nanoparticles at 10K[13]*

The magnetic properties of core/shell FePt/Fe_3O_4 nanoparticles are different from that of Au/ Fe_3O_4 nanoparticles. The core/shell FePt/Fe_3O_4 nanoparticle is a two-phase system consisting of a hard FePt phase and a soft Fe_3O_4 phase. The FePt/Fe_3O_4 core/shell nanoparticles are ferro-magnetic at low temperature but superparamagnetic at room temperature. The particles with 0.5 nm Fe_3O_4 shell have an H_c of 5 kOe, while those with 3 nm shell have an H_c value of only 1.4 kOe. The large H_c value of the core/shell nanoparticles originate from low-temperature hard magnetic properties of the FePt core.

Although they coexist hard and soft phases, the hysteresis loops measured at 10K show smooth change of magnetization with applied field, suggested that the FePt core and Fe_3O_4 shell are intimate contact and are exchange coupled. The hysteresis loop measured at 10K for

FePt/Fe_3O_4 was shown in Figure 2.7 [7, 13, 14].

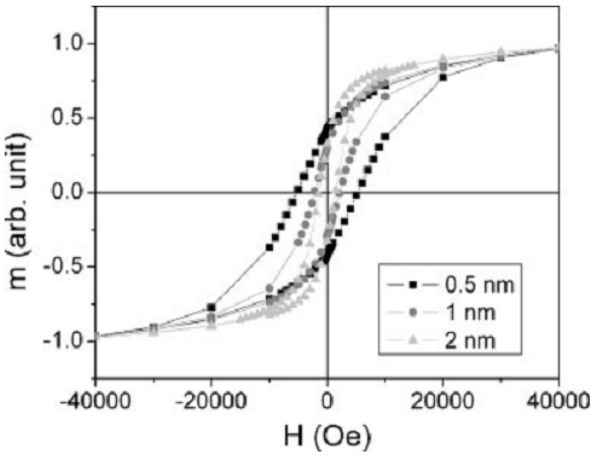

Figure 2.7 *The hysteresis loops measured at 10K for FePt/Fe_3O_4 with shell thickness changing from 0.5nm to 3 nm[14].*

Annealing of FePt/Fe_3O_4 nanoparticles was demonstrated [14]. The particles were annealed at 550℃ for 30 minutes in a mixture of hydrogen (10%) and nitrogen atmosphere. Particles with 0.5 nm Fe_3O_4 shell have coercivity value of 13.8 kOe. However, particles with 2 nm shell have a much smaller H_c value (~60Oe) than the ones with 0.5 nm shell. These results indicate the dependence of coercivity on the thickness of the Fe_3O_4 shell after annealing. The exchange coupling between the soft and hard phases can be assigned to the exchange-bias effect according to the hysteresis loop shift showed in Figure 2.8.

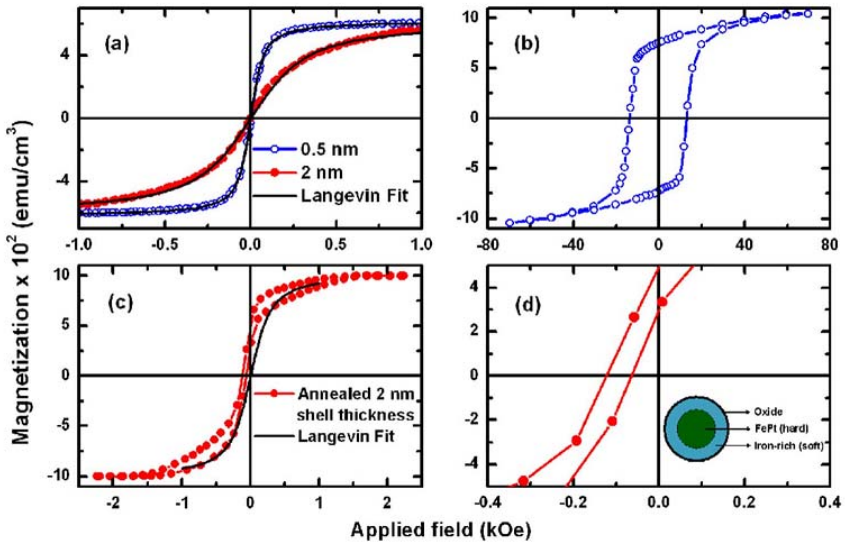

Figure 2.8 *Hysteresis loops measured at room temperature for core/shell $FePt/Fe_3O_4$ nanoparticles with different shell thickness:(a)as-synthesized and after annealing with shell thickness of (b) 0.5 nm and (c)2 nm.(d) the zoom shows that the hysteresis loops shifted, indicating the exchange bias effect[14].*

2.3 Introduction to FePt nanoparticles

2.3.1 Characteristics of FePt alloy

FePt nanoparticles possess very high magneto-crystalline anisotropy density ($Ku\sim 10^7$ Jm^{-3}) and large coercivity. This anisotropy can keep FePt nanoparticles as small as 3 nm thermally stable at room temperature. If self-assembled in a tightly packed, exchange-decoupled array with controlled magnetic easy axis direction, these FePt nanoparticles could support high-density magnetization reversal transitions and would be a candidate for ultrahigh density data storage media with potential one data bit in a single grain [15, 16].

FePt contain a near-equal atomic percentage of Fe and Pt, and includes four phases according to Fe-Pt phase diagram, which is chemically disordered face-center cubic (fcc) structure (γ phase) and chemically ordered face-centered tetragonal (fct) structure (γ_1, γ_2 and γ_3 phases).

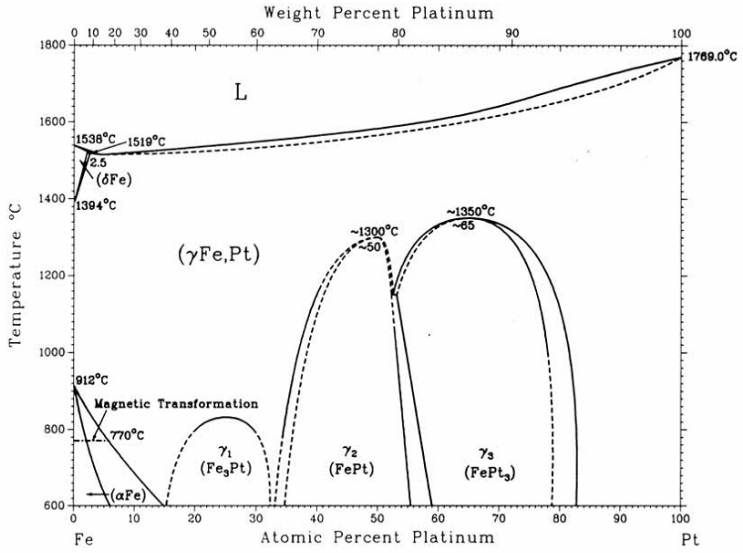

Figure 2.9 .*Phase diagram of Fe-Pt(Data are from Thaddeus B. Massalski.,Binary alloy phase diagrams, Material Park,Ohio/ASM International,1990)*

The fcc-structured FePt nanoparticles, which have a small coercivity and are magnetically soft, can be transformed to ordered fct structure by thermal annealing. Different ordered structures appear different magnetic properties. For γ_1-Fe_3Pt ($L1_2$,15 at%<Pt<30 at%), antiferromagnetism is found; for γ_2-FePt ($L1_0$,30 at%<Pt<55 at%), ferromagnetic property is found; for γ_3-$FePt_3$ ($L1_2$,60 at%<Pt<80 at%), antiferromagnetism is found.

Figure 2.10 shows the two crystal structures of FePt. The fully ordered fct-FePt can be viewed as alternating atomic layer of Fe and Pt stacked along the [001] direction. The Fe atoms occupy the sites on (0,1/2,1/2) as well as (1/2,0,1/2), and the Pt atoms occupy the site on (0,0,0) as well as (1/2,1/2,0). On the contrary, the γ phase has the atoms of Fe and Pt randomly distributed across the layer and is referred to as the chemically disordered state. The $L1_0$ phase has a tetragonal symmetry

with a lattice constant ratio (c/a) of 0.96.

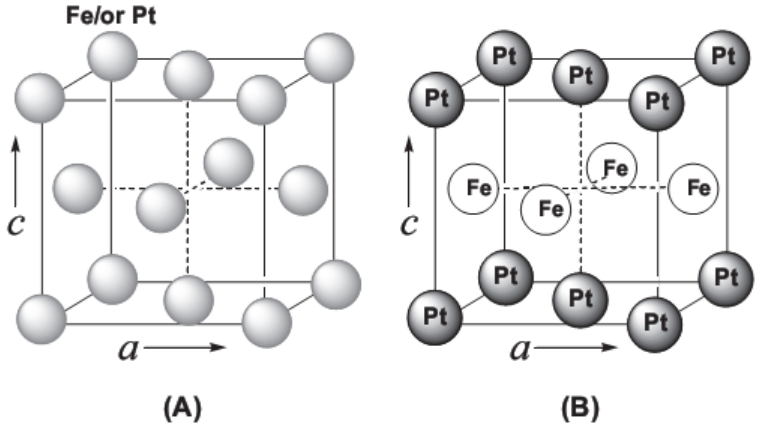

Figure 2.10 .*Schematic illustration of the unit cell of (A) chemically disordered fcc and (B) chemically ordered fct FePt[17].*

2.3.2 Synthesis of FePt nanoparticles

In 2000 year, Sun et al. successfully synthesized monodisperse FePt nanoparticles by the wet chemical method [18]. Compared with vacuum deposition techniques, chemical synthesis of FePt nanoparticles can produce greater monodispersity of grain size than the physical methods of FePt film deposition, such as sputtering. In addition, different chemical syntheses can produce nanoparticles with controlled shapes. Some groups have demonstrated syntheses for making nanocubes [19], nanorods [20], and nanowires [21].

Sun's group used 1,2-hexadecanediol to reduce the $Pt(acac)_2$ (acac=acetylacetonate, $CH_3COCHCOCH_3$) to Pt metal. Thermal

decomposition of $Fe(CO)_5$ was used to produce Fe particles, and combination of oleic acid and oleyl amine was used to stabilize the monodisperse FePt colloids and prevent oxidation. The synthetic chemistry is illustrated in Figure 2.11.

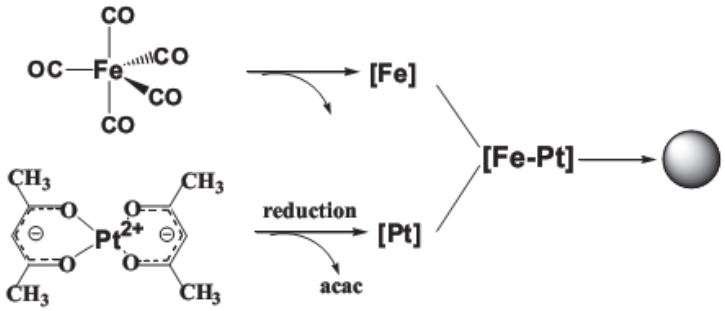

Figure 2.11 .*Schematic illustration of FePt nanoparticles formation from the decomposition of $Fe(CO)_5$ and reduction of $Pt(acac)_2$[18]*

The FePt particle size can be tuned by from 3 to 10 nm by first growing 3-nm seed particles in situ and adding more reagents to enlarge the existing seeds to the desired size, and the standard deviation is less than 5%.

FePt particle size could be controlled with 1 nm accuracy by changing several synthetic parameters, including precursors, solvents, amount of surfactants, and heating rate of the solution [22]. Surfactants typically play an important role in controlling the size and shape of FePt nanoparticles. The effect of the molar ratio of the surfactants to $Pt(acac)_2$ on the size of FePt particles was observed [22, 23]. FePt nanoparticles with average size of 4 nm were obtained when the molar ratio of surfactants to $Pt(acac)_2$ was 1. By decreasing the molar ratio up to 0.75, the particles size decreased to 3 nm. By increasing the ratio up to 10, the

particle size increased to 9 nm. It is suggested that the particle size increases with increasing surfactant concentration. It is believed that the increase in the surfactant amount resulted in the formation of stable complexes with individual metal atoms of the precursors. As a result, an increase in surfactant concentration is expected to suppress the nucleation process and larger particles are produced. The relationship between the particle size, the ratio of surfactants to Pt precursor, and heating rate was shown in Figure 2.14.

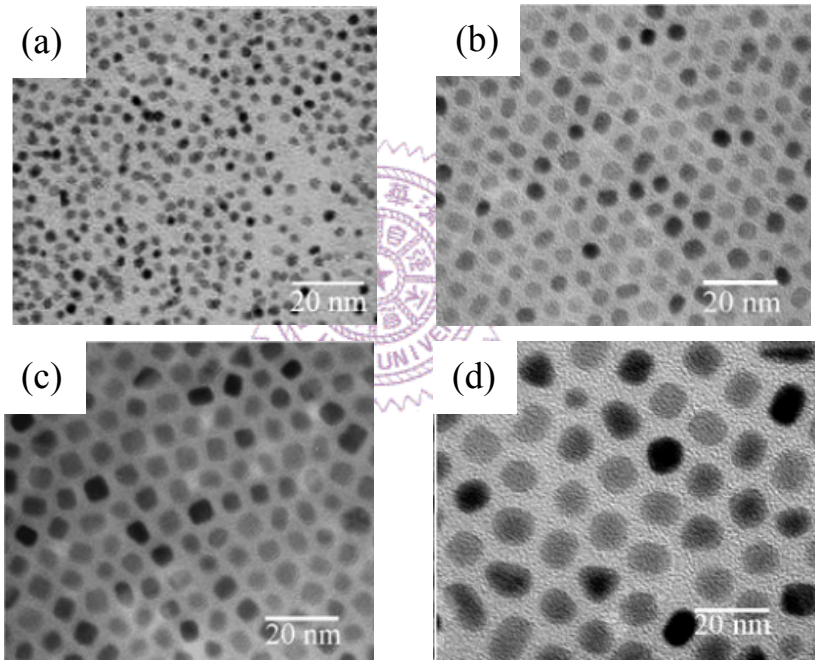

Figure 2.12 .*TEM images of as-synthesized FePt nanoparticles of size (a)3 nm,(b) 5nm, (c) 7 nm, (d) 9nm[22]*

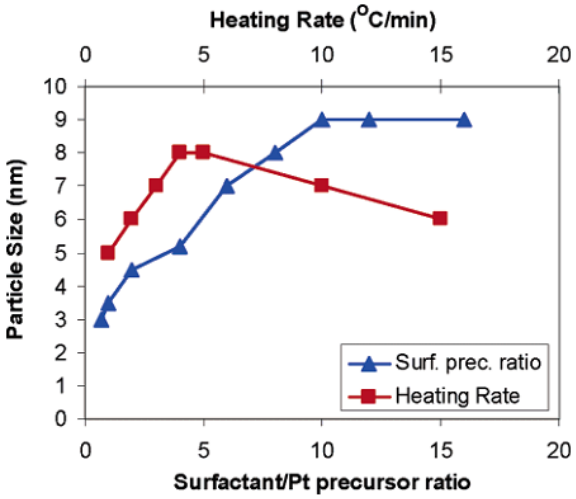

Figure 2.13 *Heating rate and surfactant/Pt precursor dependence on particle size[22]*

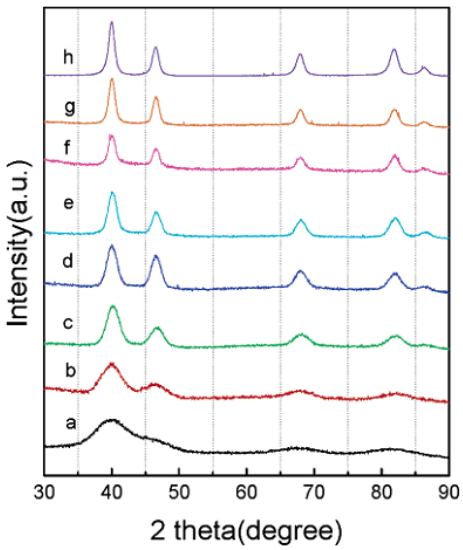

Figure 2.14 *XRD of as-synthesized FePt nanoparticles with different sizes[22]*

The heating rate of reaction also affects the particle size. As the heating rate was increased from 5 to 15℃/min, the average particle size was decreased from 8 to 6nm, respectively. With the increase in the heating rate, the nucleation rate was increased. Due to the enhanced nucleation rate, more nuclei were formed at the initial stage. However, when the heating rate is very slow, competition between the nucleation

and the growth occurs and smaller particles may be produced. Reducing agents also affected the size of FePt nanoparticles.

It is found that the extra reducing power introduced by the agent could lead to facile reduction of $Pt(acac)_2$ to Pt, resulting in fast nucleation of FePt and consumption of metal precursors, and as a result, smaller sized particles. The absence of additional reducing agent in the reaction mixture might slow the nucleation rate, allowing more metal precursors to deposit around the nuclei and leading to larger particle size [24]. However, fine tuning of the particle size remains a challenging task.

2.3.3 Shape control of FePt nanoparticles

The potential advantage of shape controlled FePt nanoparticles for high density magnetic recording media is that their high magneto-crystalline anisotropy and shape anisotropy allow alignment of their magnetic easy axis when deposited in self-assembly films. The shape could be controlled by varying the compositions of FePt nanoparticles and synthesis methods. However, the challenge is that it is not easy to control both the composition and shape of alloy nanoparticles.

The cubic FePt nanoparticles were first synthesized by Shukla et al.[19], Fe generated by decomposition of $Fe(CO)_5$ is used as a reducing agent for $Pt(acac)_2$. A solution of $Pt(acac)_2$ (0.5mmol), $Fe(CO)_5$ (0.5mmol),oleic acid(4 mmol), and oleylamine (4 mmol) in dichloroben-

zene was heated at 4℃/min until the reflux temperature of 170℃ was achieved. The reaction mixture was then refluxed at 170℃ for 24h. Figure 2.15 shows FePt nanoparticles that are roughly cubic in shape.

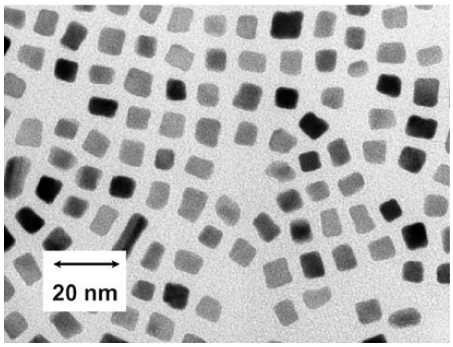

Figure 2.15 *TEM image of FePt nanocubes[19]*

Chen et al. have demonstrated the FePt nanocubes as well [25]. However, their synthesis method is totally different from N. Shukla's group. According to their studies, FePt nanocubes could be prepared by controlling the addition sequence of the stabilizers, oleyl- amine and oleic acid. Pt is generated from the reduction of $Pt(acac)_2$; Fe is generated from the decomposition of $Fe(CO)_5$. The key to the success of the nanocubes synthesis is that the reaction temperature is at 205℃, rather than 300 ℃, the temperature used for FePt nanoparticles synthesis. The TEM picture of FePt nanocubes is shown in Figure 2.15.

It is believed that the nanocubes are formed from the growth of the cubic Pt-rich nuclei generated during the initial stage of the reaction. In a kinetic growth, the Fe-rich species prefer to deposit on the (100) plane, leading to the formation of cubes. If oleyl amine is added first,

sphere-like FePt nanoparticles are separated. This indicates that the amine reacts with Pt, forming stable Pt-NH_2-complex and hindering the nucleation process. The uniform FePt nanocubes must be derived from atomic diffusion between Pt-rich core and Fe-rich shell.

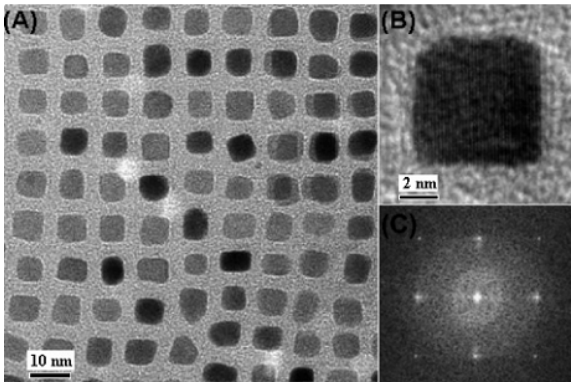

Figure 2.16 *TEM image of (A) 6.9 nm FePt nanocubes; (B)HRTEM of a single FePt nanocubes;(C) FFT of the cube in (B)[26]*

The shape of FePt nanoparticles could be varied by using different solvents. N Shukla et al. studied the effect of different solvents on the shapes, sizes, and compositions of FePt nanoparticles [26]. The specialty of this work is that a high pressure cell was used for the synthesis, so all the reaction temperature is the same (270℃) independent of the boiling points of the solvents. Table 2.2 shows the relation between the solvents and the sizes of FePt nanoparticles.

Table 2.2 *The relationship between the reaction mixture and products[26]*

Shape	Compos.	Temp. (°C)	Pressure (bar)	Solvent	Reactant/surfactant
Spherical	$Fe_{50}Pt_{50}$	280	1	Dioctylether (Octyl ether)	0.0005 m $Pt(acac)_2$ 0.0005 m $Fe(acac)_2$ 0.0005 m oleylamine 0.0005 m oleic acid
Hexagonal	$Fe_{18}Pt_{82}$	270	22 [8]	2 ml toluene	0.00005 m $Pt(acac)_2$ 0.00008 m $Fe(CO)_5$ 0.0006 ml oleylamine 0.0006 m oleic acid
Rods	$Fe_{26}Pt_{74}$	270	6 [9]	20 ml 1,2-dichlorobenzene	0.0005 m $Pt(acac)_2$ 0.0009 m $Fe(CO)_5$ 0.009 m oleylamine 0.009 m oleic acid
Wires	$Fe_{50}Pt_{50}$	270	2	24 ml oleylamine	0.0005 m $Pt(acac)_2$ 0.0009 m $Fe(CO)_5$
Cubes	$Fe_{97}Pt_3$	270	6 [9]	20 ml 1,2-dichlorobenzene	0.0005 m $Pt(acac)_2$ 0.0009 m $Fe(CO)_5$ 0.006 m oleylamine 0.006 m oleic acid

Variation of both nanoparticles size and shape has been achieved by using various different solvents. The solvents used in the nanoparticle synthesis can influence the product because they can play a role as surfactants. Using solvents of various types it has been possible to synthesize Fe_xPt_{100-x} nanoparticles with a variety of shapes including spherical, rod-like, cubic, hexagonal and high aspect ratio wires (Figure 2.17) . Control of nanoparticle shape opens the door to their being used in various technological applications for which spherical nanoparticles are ineffective.

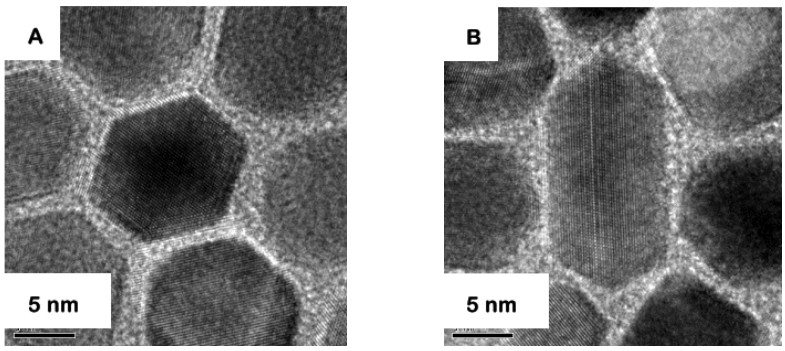

Figure 2.17 *HRTEM image of hexagonal $Fe_{18}Pt_{82}$ nanoparticles synthesized in a toluene at a pressure of 22 bar and a temperature at 270 ℃*

2.3.4 Annealing effects on FePt nanoparticles

As-synthesized FePt nanoparticles are chemically disordered face-centered cubic (FCC) phase which does not provide the high magneto- crystalline anisotropy. To transform the chemically disorder phase to chemically ordered $L1_0$ phase with face-centered tetragonal (fct) structure, a post annealing process is required. During annealing, both agglomeration and sintering of nanoparticles become a problem. To solve these problems, some efforts have been made to obtain monodisperse fct FePt nanoparticles. The following are some methods that can improve the problem.

(1) The use of high boiling point solvents in the polyol process. In this approach, higher synthesis temperatures allow the formation of FePt nanoparticles partially transformed to fct phase [27].

(2) Coating the fcc FePt nanoparticles with high-melting-point materials and annealing the mixture to obtain fct FePt nanoparticles. The advantage is that high temperature could be carried out without sintering. an immiscible silica matrix [28], linker molecules(polyethylenimine,(PEI) and 3-aminopropyldimethy-ethoxysilane(APS)) [29],TiO_2 matrix [30], SiO_2 shell [31], and MgO shells [32] are used as coating materials. However, the coating materials are not easy to remove after annealing.

(3) Salt matrix annealing was proposed [33]. The ball milled salt powders are mixed with the as-synthesized particles before

annealing at high temperature. The salts are then removed by washing the sample in water. The advantage is that the salt is easy to be removed and get the monodisperse fct FePt nanoparticles.

(4) Lower the ordering temperature by doping some elements, such as Ag, Au, and Cu in the FePt nanoparticles [34].

(5) Other approaches, such as rapid thermal annealing [35] and pulse laser annealing [36], are tried.

Because salt-matrix annealing is a simple and useful method, I will pick up the method in my work. We focus on the magnetic properties and morphology of FePt nanoparticles by salt-matrix annealing. Figure 2.18 shows the TEM images of the 4 and 8 nm as-synthesized fcc FePt nanoparticles and annealed fct particles at 750℃ [37].

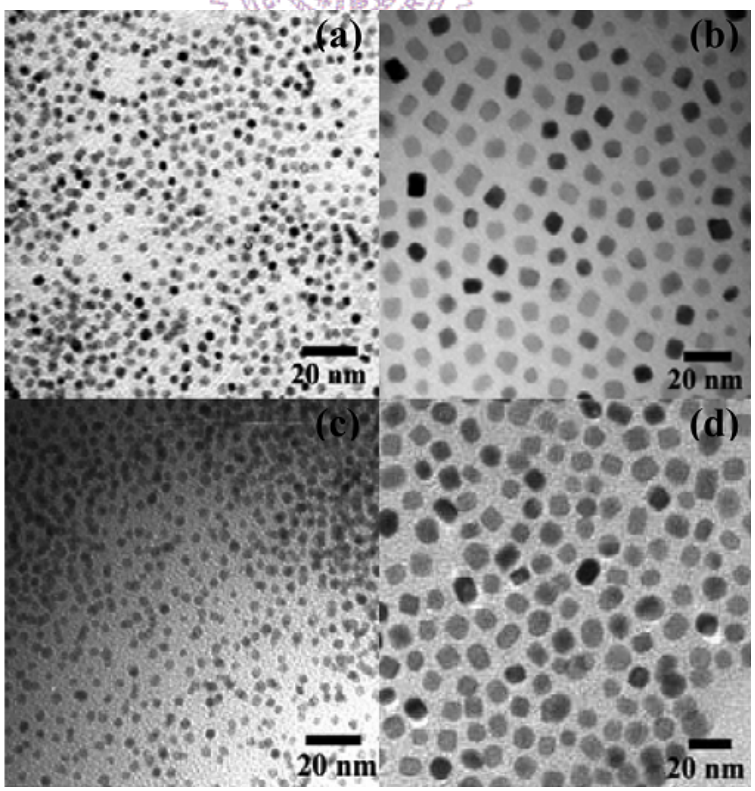

Figure 2.18 *(a) and (b) are the TEM images of as-synthesized FePt*

nanoparticles. (c) and (d) are the annealed particles from (a) and (b) at 700℃ for 4h[37].

From the above TEM images, we can see that the particle sizes still retain. It is suggested that this method can prevent particles from sintering and growth through high-temperature annealing. Beside, the salt to particle ratio has to be higher than 20:1. The lower salt ratios gave significant particle sintering and agglomeration. Annealing at higher temperatures and extended time should be accompanied with higher salt to FePt ratio in order to avoid sintering.

The annealed fct FePt nanoparticles were mixed with epoxy to measure their magnetic properties. Figure 2.19 shows the hysteresis loops of the fct nanoparticles annealed in different conditions. The particles exhibited giant coercivity up to 30kOe at room temperature. It can be seen that the hysteresis loops of the 4 nm particles show kink after being annealed for 8 h. this may be attributed to the size dependence phase-transition behavior. In the relatively small nanoparticles, the transition in not as complete as in large in large particles which give the two-phase behavior as shown by the loops.

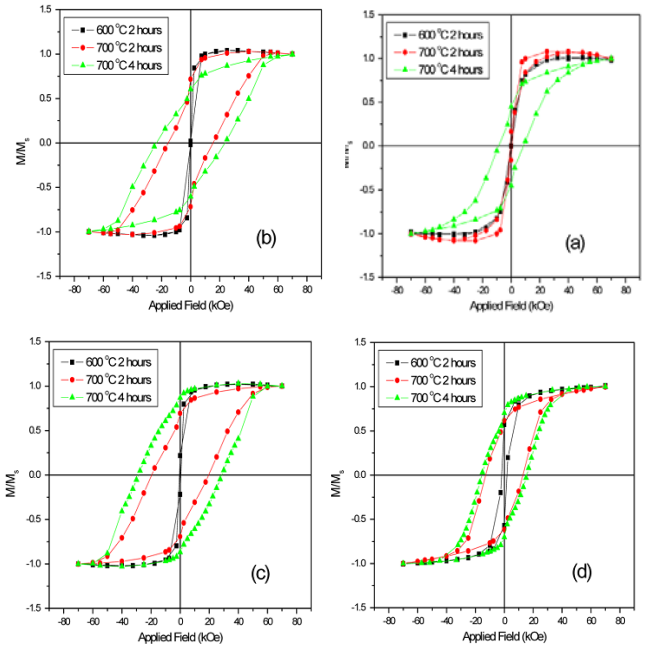

Figure 2.19 *Hysteresis loop of FePt nanoparticles with sizes of (a) 4, (b) 6, (c) 8, and (d) 15 nm annealed in different conditions[37].*

2.4 Introduction to Magnetite

2.4.1 Properties of Magnetite

Magnetite (Fe_3O_4) has a common iron oxide that has a cubic inverse spinel structure. The inverse spinel structure is constructed of face-centered cubic packed lattice of oxygen atoms with the tetrahedral sites (T_d) occupied by Fe^{2+} ions and octahedral sites (O_h) occupied by Fe^{2+} and Fe^{3+} . Under an external magnetic field, the magnetic spins of the ions at the O_h sites align parallel to the external magnetic field but those at the T_d sites align antiparallel to the field, shown in Figure 2.20.

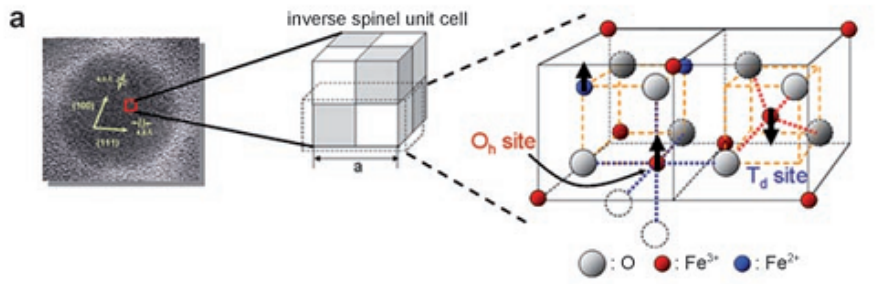

Figure 2.20 *Metal ferrite nanoparticles with inverse spinel structure and is ferromagnetic spin alignments; O_h: octahedral hole; T_d : tetrahedral hole.* [38]

Since Fe^{2+} has a d^6 configuration and Fe^{3+} has a d^5 configuration with a high state, the total magnetic moment per unit $(Fe^{3+})_{Td}(Fe^{2+}\ Fe^{3+})_{Oh}O_4$ is 4 μ_B. The compound has unique electric and magnetic properties due to

the transfer of electrons between Fe^{2+} and Fe^{3+} in the octahedral sites.

Magnetite is expected to half-metallic material which is metallic for one-spin directional electrons and insulating for the other. The magnetite undergoes a metal-insulator transition at temperature of about 120K, called Verwey transition [39]. Some investigations indicate that the nature of the Verwey transition and magnetic properties are related to the metal-to-oxygen stoichiometry [40]. Below the Verwey transition, single crystals [41] and expitaxial films [42] have been observed to exhibit larger negative magnetoresistance. However, the phenomenon is unclear on the nanoparticles in that compact nanoparticles provide a lot of grain boundary, which is the origin of electron scattering [43].

2.4.2 Synthesis of Magnetite Nanoparticles

Fe_3O_4 nanoparticles are commonly produced through coprecipitation of ferrous (Fe^{2+}) and ferric (Fe^{3+}) ions by a base solution, such as NaOH, or $NH_3 \cdot H_2O$ in an aqueous solution [44]. They also are produced by thermal decomposition of alkaline solution of Fe^{3+} chelate in the presence of hydraze and by sonochemical decomposition of hydrolyzed Fe^{2+} salt followed by thermal treatment [45]. However, the disadvantage of these aqueous-solution syntheses is that the pH value of the reaction mixture has to be adjusted in both the synthesis and purification. It is more difficult to control the synthetic parameters.

Here we focus on the organic-phase synthesis of Fe_3O_4 nano-

particles[46]. Sun et al. first demonstrated the synthesis of Fe_3O_4 nanoparticles through the organic solution-phase decomposition of $Fe(acac)_3$ at high temperature. The author demonstrated the high-temperature (265 ℃) reaction of $Fe(acac)_3$ in the phenyl ether in the presence of alcohol, oleic acid, and oleyl amine can be used to produce monodisperse magnetite nanoparticles. The Figure 2.21 showed the procedure of synthesis of Fe_3O_4 nanoparticles. In order to get larger Fe_3O_4 nanoparticles, they used seed-mediated growth method [47] . The smaller Fe_3O_4 nanoparticles were mixed with more precursor materials, and the mixture was heated as in the synthesis of smaller nanoparticles. In order to get monodisperse Fe_3O_4 nanoparticles, the key is to heat the mixture to 200℃ first and remain at that temperature for some time before it is heated to reflux at 265℃ in phenyl ether of at 300℃ in benzyl ether (Figure 2.21) [48].

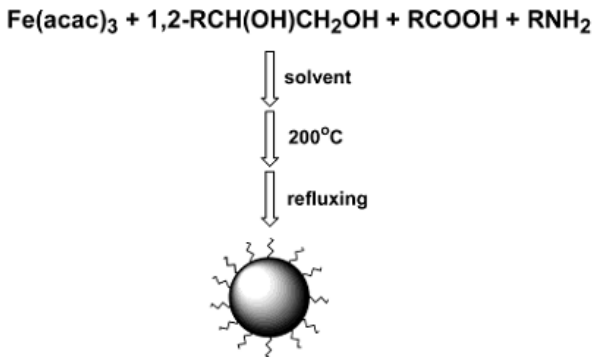

Figure 2.21 *The illustration of forming Fe_3O_4 nanoparticles[48]*

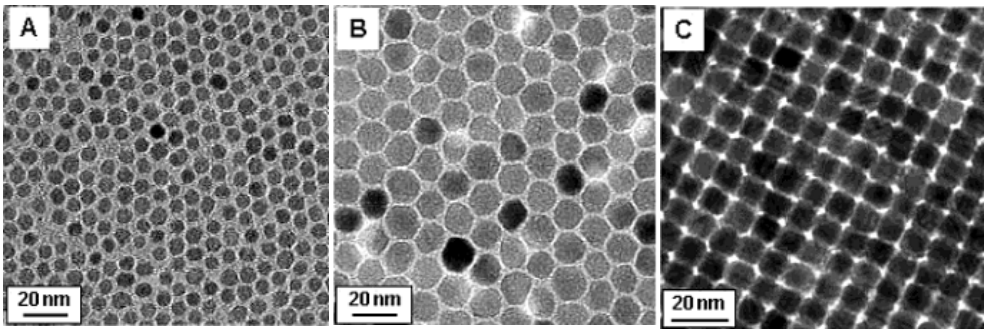

Figure 2.22 *TEM images of (A)6 nm and (B) 12nm Fe_3O_4 nanoparticles. (C)3D superlattice of 10 nm Fe_3O_4 nanoparticles[48].*

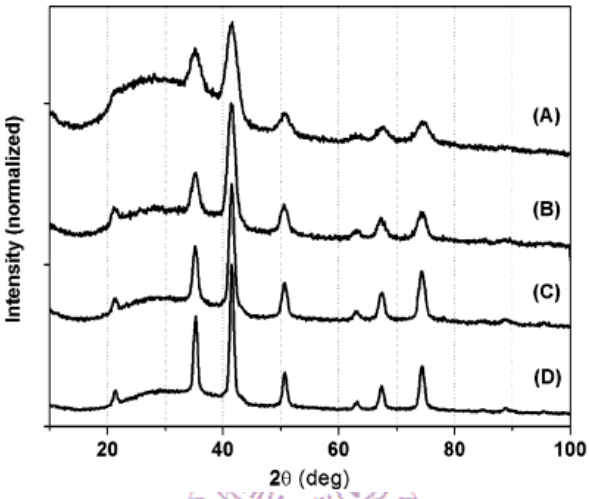

Figure 2.23 *XRD of (A)4 nm,(B) 8 nm,(C) 12 nm and (D) 16 nm Fe_3O_4 nanoparticle assemblies[48].*

Magnetic measurements on all Fe_3O_4 nanoparticles indicate that the particles are superparamagnetic at room temperature, meaning that the thermal energy can overcome the anisotropy energy barrier of a single particle, and the net magnetization of the particle assemblies in the absence of an external field is zero. Figure 2.24 shows the hysteresis loops of 16 nm Fe_3O_4 nanoparticles measured at both 10 K and room temperature. It can be seen that the particles are ferromagnetic at 10 K with coercivity of 450 Oe.

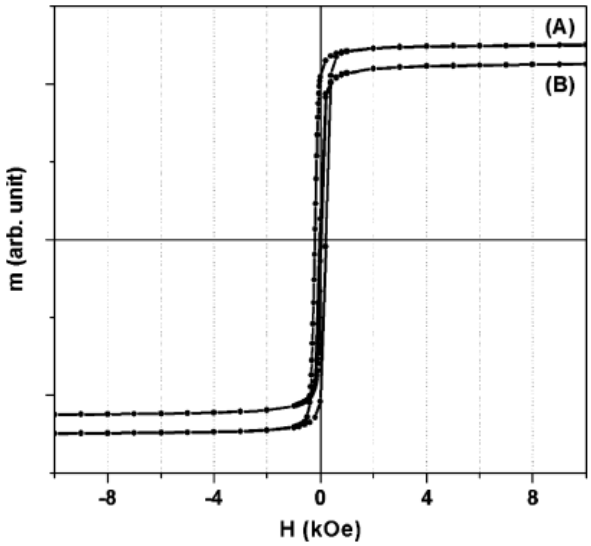

Figure 2.24 *Hysteresis loops of the 16 nm Fe_3O_4 nanoparticles assembly measured at (A) 10 K and (B) 300 K.*

2.4.3 Shape-Controlled Synthesis of Magnetite Nanoparticles

Controlling the shape of magnetic nanoparticles is attractive because the shape may lead to anisotropic magnetic properties of the nanoparticles. Besides, nanoparticles with different shapes could be used as building blocks to control the crystal orientation of the nanoparticles in an assembly. When the magnetic easy axis of a particle correlates with its crystal structure, the shape-induced crystal orientation of each particle in an assembly would lead to an aligned magnetic easy axis. Such alignment is useful for the application on the data storage.

In 2004, cubelike $MnFe_2O_4$ nanoparticles were demonstrated [49]. The paper mentioned that the shape could be controlled by the amount of stabilizers added to the reaction mixture. When the surfactant/$Fe(acac)_3$

ratio is smaller than 3:1, the particles are nearly spherical with no well-defined facets. Increasing the ratio to 3:1 yields cubelike particles. If the particles are prepared by seed-mediated method, polyhedron-shaped particles are obtained. Self-assembly of these shaped particles can lead to crystal orientation of each particle in a self-assembly superlattice, showed in Figure 2.25.

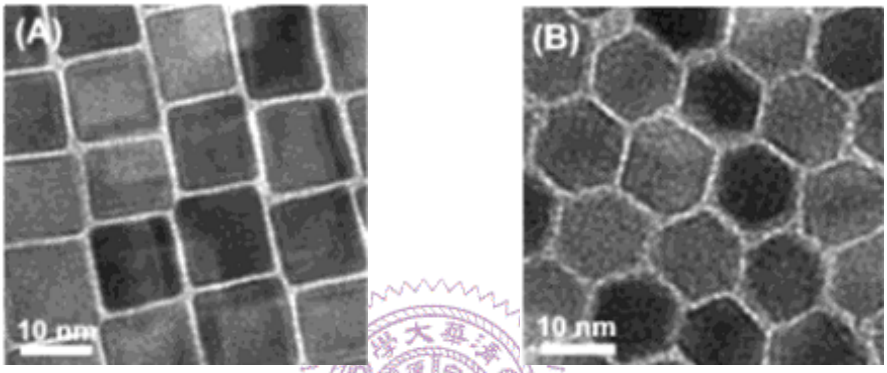

Figure 2.25 *TEM images of 12-nm cubelike and polyhedron-shaped $MnFe_2O_4$ nanoparticles[48]*

From the XRD (Figure 2.26), self-assembly cubelike particle on Si(100) substrate shows the intensity (400) peak, and that of polyhedron-shaped particles reveals two strong reflections from (220) and (400). They are quite different from that of a 3D randomly oriented spinel structured $MnFe_2O_4$ nanoparticles assembly, which shows a strong (311) peak. Cubelike particles assembly shows a strong (400) peak indicates that each of the cubelike particles in the cubic assembly has preferred crystal orientation with [1] planes parallel to the Si substrate, while for the polyhedron-shaped particle assembly, the {110} planes are parallel to

the substrate.

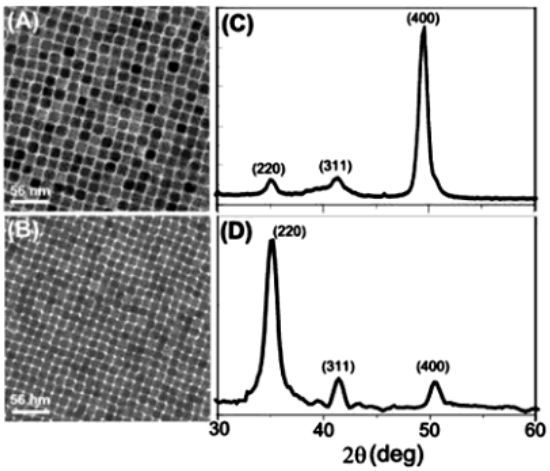

Figure 2.26 *(A) and (B) are the TEM images of 12 nm $MnFe_2O_4$ of cubelike and polyhedron-shaped nanoparticles. (C) and (D) are the XRD data corresponding to the left images[48].*

Some groups change the reactants to obtain the cubic shapes. Iron oxide nanocubes were obtained in the presence of sodium oleate(Figure 2.27) [50]. In contrast, using oleic acid and dibutylammonium oleate (DBAOL) induces growth of monodisperse spherical particles.

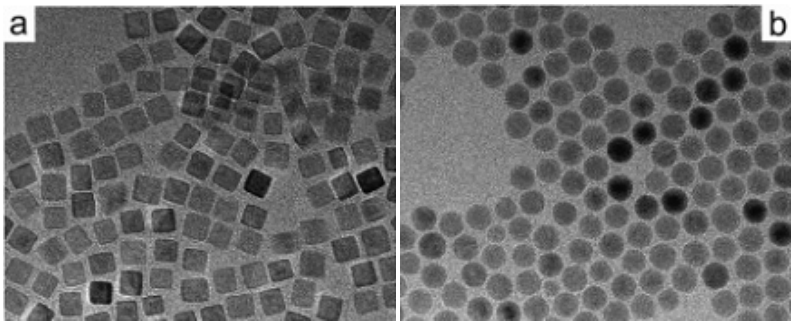

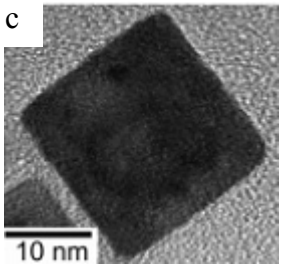

Figure 2.27 *TEM images of cubic and spherical iron oxide nanoparticles*

It is believed that the cubic shape of the iron oxide is a result of a slower growth rate for the {100} faces compared to all other facets. The difference on the growth rate can be attributed to a different adhesion of the stabilizer on the growing surface. Takahashi et al. further improved that different surfactants can change the shape of the particle [51]. When the molar ratio of oleic acid(OA) to $Fe(acac)_3$ was increased to 4 , the molar ratio of oleyl amine and 1,2-hexadecandiol to $Fe(acac)_3$ was reduced .The cubelike Fe_3O_4 can be obtained. In this way, they could obtain magnetite nanocubes. Such a modification based on the OA with a carboxylic group, -COOH, has a selective binding onto different energy crystal facets together with a nonpolar tail group for steric hindering. However, oleyl amine with a $–NH_2$ group has a weak and isotropic binding onto the surface of the particle.

The growth mechanism was further reported by T. Hyeon et al. [52]. Under their synthetic condition, when the amount of benzyl ether was reduced and the reaction time was increased to 1h, ~110 nm particles composed of truncated cubes and truncated octahedral were obtained. By increasing the reaction time to 1.5 h and 2 h, the particle grew to larger

and more perfect cubic shapes. Based on the HRTEM (Figure 2.28), the author found that the nanocubes are formed as a result of fast growth along <111> directions, and the surfaces to the final nanocubes correspond to {100} planes. The overall shape evolution is illustrated in Figure 2.29. Kinetically controlled growth under high monomer concentration seems to be responsible for this anisotropic growth.

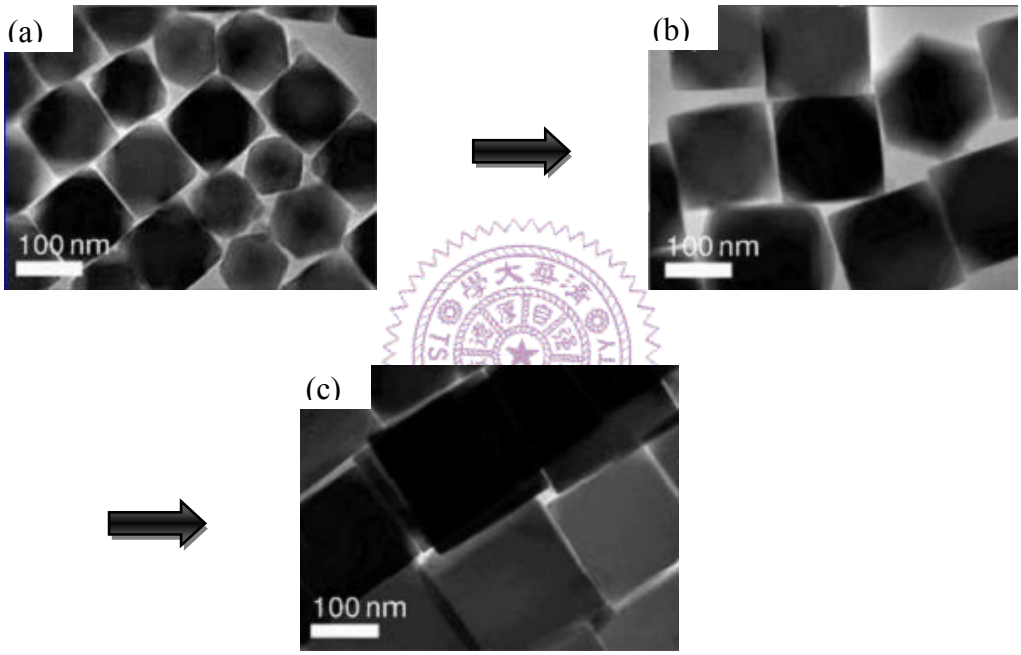

Figure 2.28 *TEM images of (a) and (b) are the truncated octahedral nanoparticles. (c) is 160 nm nanocubes[52].*

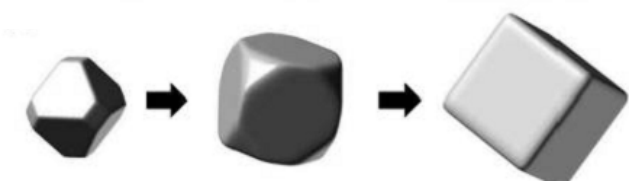

Figure 2.29 *The overall shape evolution of the Fe_3O_4 nanoparticles[52]*

The magnetic properties of Fe_3O_4 nanocubes are a soft ferromagnetic

material with high saturation and low coercivity, the same as spherical Fe_3O_4 nanoparticles.

Chapter 3 Experimental Design and Analysis Technique

3.1 Experimental procedures

This chapter will include the part of experiment and principal of analysis equipments, which were performed on my thesis. In my thesis, the experimental steps were followed by Sun et. al [18] with some modification. The following shows the procedures of experiments.

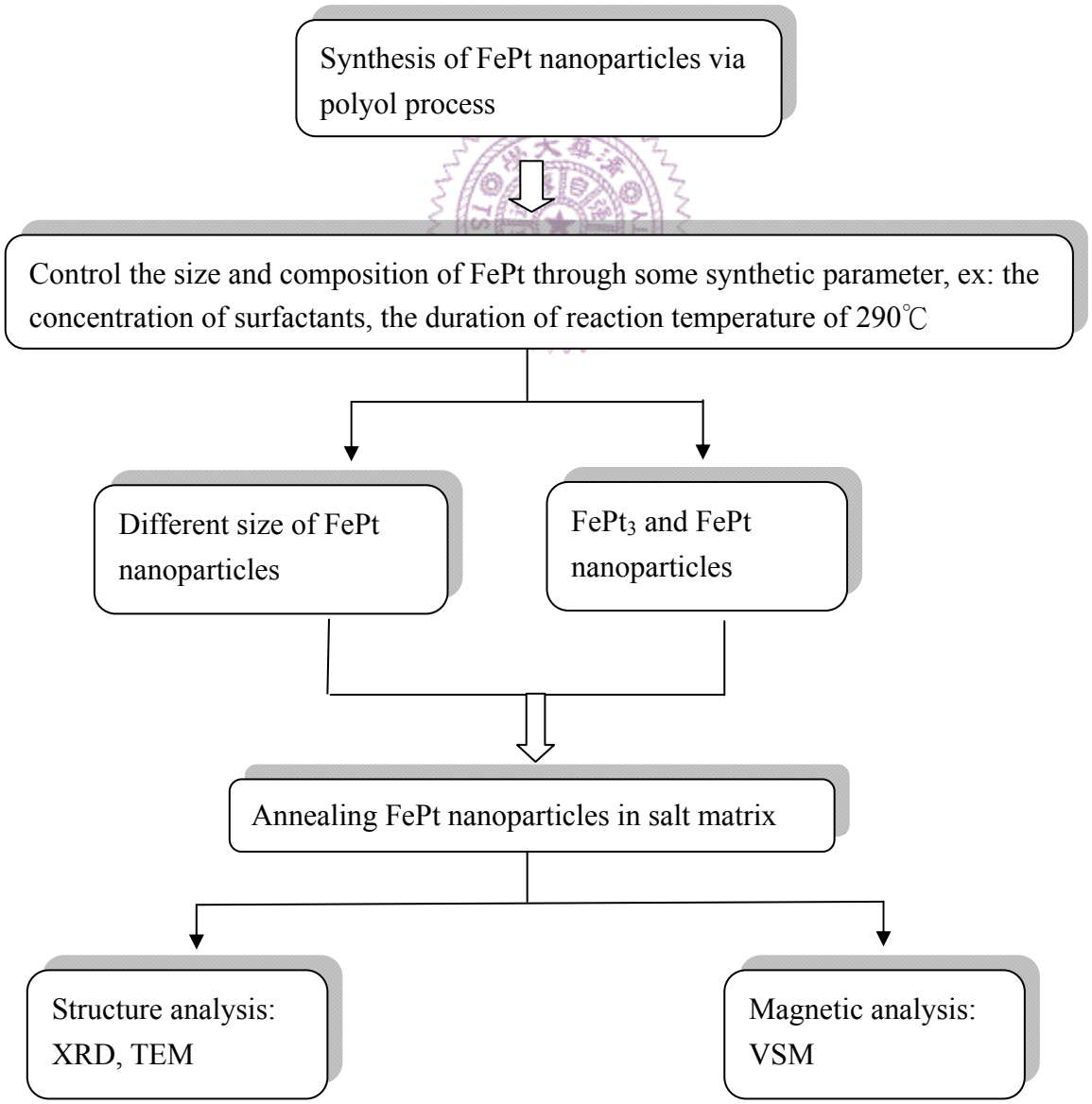

3.2 Experimental Design

3.2.1 The apparatus of experiment

The synthetic experiments were carried out using standard airless technique in argon atmosphere, and the apparatus of synthetic process is illustrated by Figure 3.1.

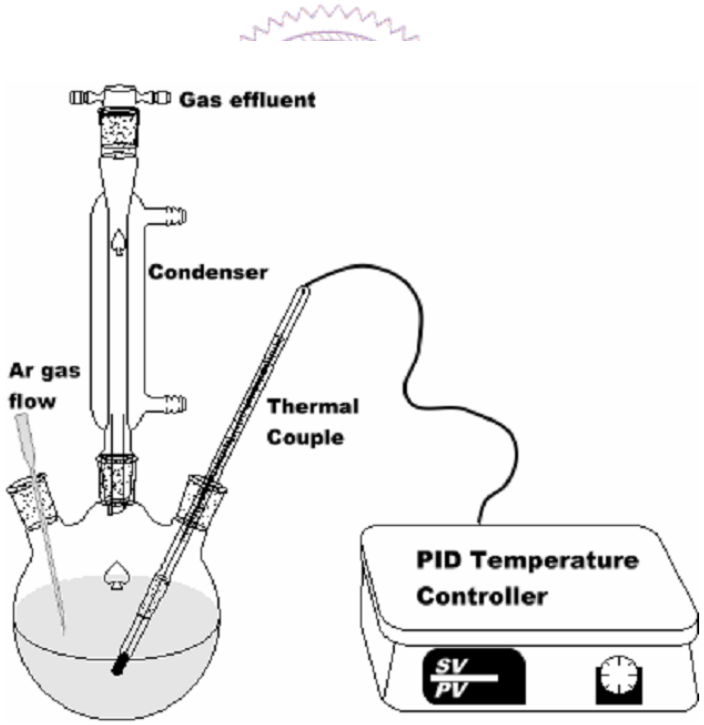

Figure 3.1 *The apparatus of the synthesis*

3.2.2 Reagent list

reagent	function
platinum acetylacetonate,$Pt(acac)_2$	The precursor of Pt
Iron pentacarbonyl,$Fe(CO)_5$	The precursor of Fe
Benzyl ether	Solvent,T_b = 297℃
1,2-hexadecanediol	reduction
Oleic acid	Surfactant, stabilizer
Oleyl amine	Surfactant, stabilizer

3.2.3 Procedures of experiment

Preparation of fcc-FePt nanoparticles

1. A mixture of $Pt(acac)_2$, 1,2-hexadecanediol, oleic acid, and benzyl ether was heated to 110℃ in a three-necked round-bottom flask under a argon atmosphere. A designed amount of $Fe(CO)_5$, oleyl amine were injected into the solution through a syringe at 110℃ and then the mixture was heated to reflux(290℃) for 30 minutes.
2. The heat source was then removed and the reaction mixture was allowed to cool to room temperature.
3. The black products was precipitated by adding ethanol and separated by centrifugation. The yellow-brown supernatant was discarded. The black precipitate was dispersed in hexane in the excess of oleic acid and oleyl amine.

As-synthesized FePt nanoparticles annealed with NaCl

1. The salt powders were ball milled for more than 24 h to reach particle size smaller than 20 μm before they were mixed with the fcc FePt nanoparticles.
2. The fcc FePt nanoparticles with different size (3~6nm) were mixed with a great quantity of NaCl. The mixture was then annealed at temperature of 800℃ for 1 h under the forming gas (10%H_2 +90% Ar).
3. After annealing, the salts were removed from the samples by washing the mixture in deionized water followed by centrifugation. Water was decanted from the centrifuge tube and then the previous step was prepared again to ensure that the salt was completely removed from the samples.
4. The remaining particles were rinsed with hexane, oleic acid, and oleyl amine and were centrifuged again. Dispersions of FePt nanoparticles were eventually obtained in hexane.

3.3 Analysis equipments

3.3.1 Vibrating Sample Magnetometer (VSM)

The measurement method was proposed by Foner. The principle of VSM is that the sample which vibrates near the coil would induce the

variation of magnetic flux. The measured sample can be in the shape of rod or sheet and is mounted on one end of the test rod. The other end of the test rod is connected to loudspeaker. In the beginning with measuring, the testing rod vibrates together with sample with 80Hz frequency. The direction of vibration is perpendicular to the magnetic field. Because the sample vibrates in a magnetic field which induces a variation of magnetic flux though the detection coils, an induced electromotive force would be formed in the coils. With a reference sample (saturation moment M_s is known) fixed at the testing rod vibrating together with the measured sample, there is also an induced electromotive force formed in the reference coils. Therefore, we can compare the difference of induced electromotive force in the detection coils and reference coils to obtain the magnetic moment of measured sample. The scheme of VSM is illustrated in Figure 3.2.

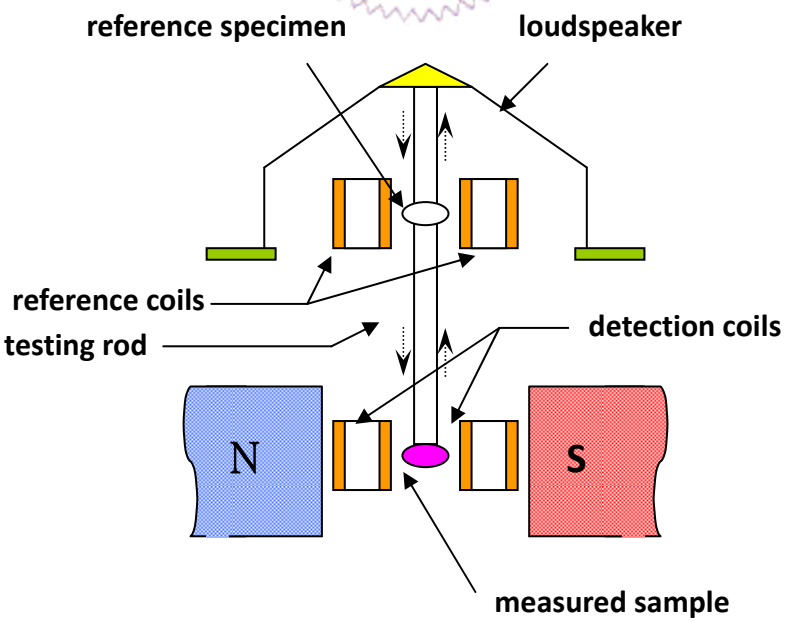

Figure 3.2 *Schematic illustration of VSM.*

3.3.2 X-Ray Diffraction (XRD)

The essential features of XRD instrument is shown in Figure 3.3. The rotating axis of specimen and detector are defined as θ and 2θ axis respectively. The detector can be rotated about sample and set at any desired angular position. The crystal is usually cut or cleaved so that a particular set of reflecting planes of known spacing is parallel to its surface, as suggested by the drawing. In use, the specimen is positioned so that its reflecting planes make some angle θ with the incident beam, and the detector is set at the corresponding angle 2θ. The intensity of the diffracted beam is then measured and its wavelength calculated from the Bragg law "$2d\sin\theta=n\lambda$", this procedure being repeated for various angles θ.

The directions in which a beam of given wavelength is diffracted by a given set of lattice planes are determined by the crystal system to which the crystal belongs and its lattice parameters. This is an important point and so is its converse: all we can possibly determine about an unknown crystal by measurements of the directions of diffracted beams are the shape and size of the unit cell. In addition, the intensities of diffracted beams are determined by the positions of atoms within the unit cell.

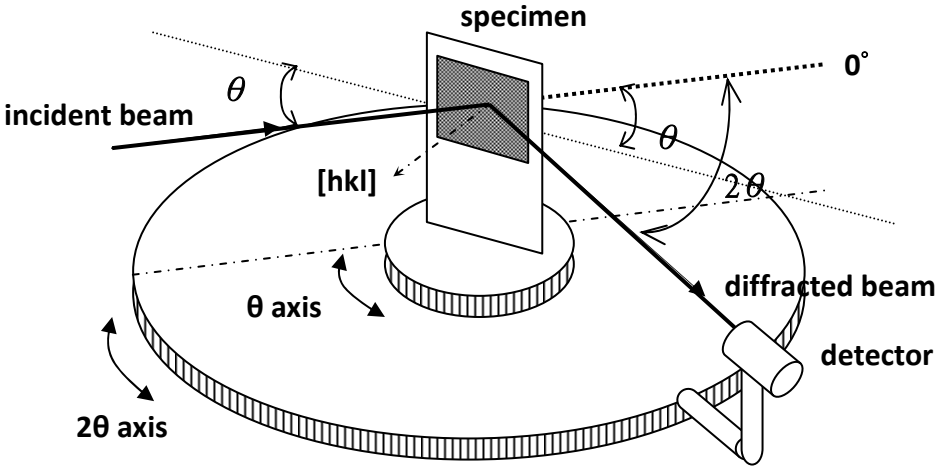

Figure. 3.3 *XRD spectrometer.*

3.3.3 Transmission electron microscope (TEM)

TEM studies were conducted using a Jeol JEM-1400 microscope operating at 120KeV with a Gatan CCD camera. The equipment can be divided into four parts: (1) the source of the electron beam, (2) the electromagnetic lens system. Several lens are indicated and driven by Lorentz force to focus electron beam, (3) specimen room, and (4) signal process system. On the bottom of TEM column is comprised of screen

and some detector for energy analyzer.

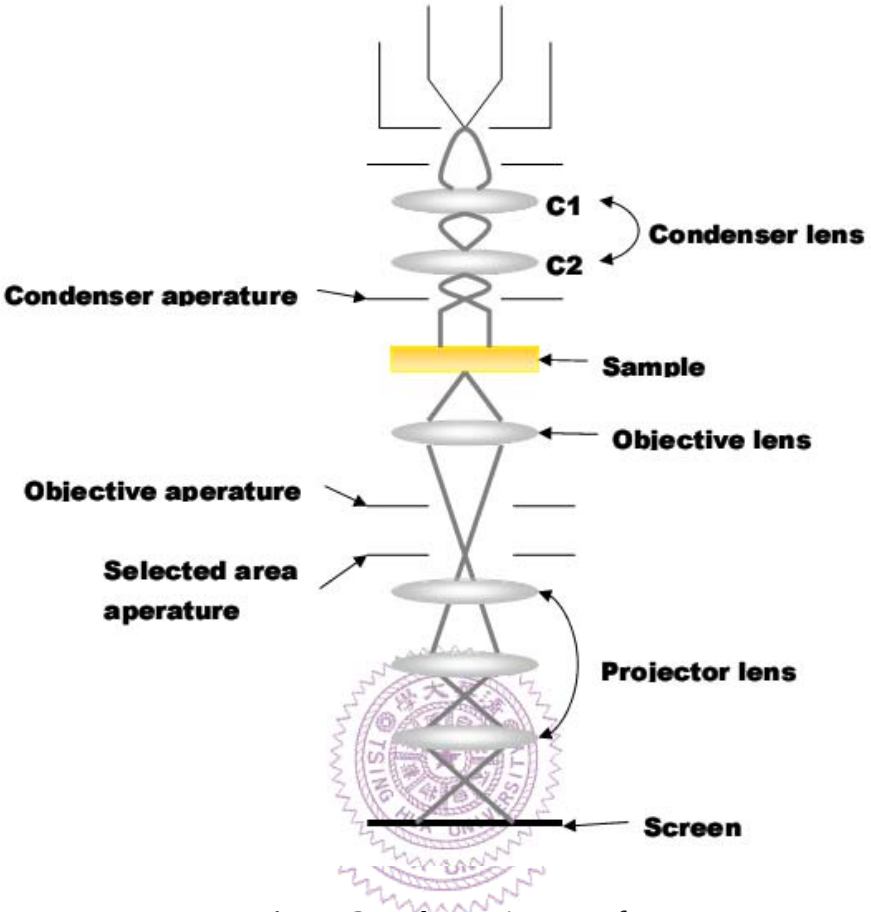

Figure 3.4 *The equipment of TEM*

Chapter 4 Results and Discussion

This chapter is organized into three sections. The first section is controlling size distribution and composition of FePt nanoparticles by thermodecomposition method. Second section is focused on the study of salt matrix-aid effect in annealing steps of as-synthesized FePt nanoparticles and the magnetic properties of annealed FePt alloy. The exchange coupling phenomenon between FePt (FM) and $FePt_3$ (AFM) nanoparticles was demonstrated and discussed in the final section.

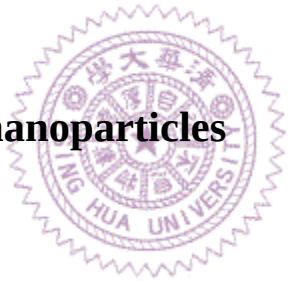

4.1 Synthesis of FePt nanoparticles

Tuning the size in the desired range along with tight control on composition of FePt nanoparticles has been an attractive field in material science. Particle size smaller than 6 nm with well size distribution and Fe/Pt ratio control have been reported[53]. However, FePt with larger size are rarely discussed due to the difficulty in synthesis of uniform nanoparticles with desired composition. Herein, we present a one-step synthesis of FePt nanoparticles with the controlled composition and tunable size up to 8 nm in diameter. The effects of the concentration of the surfactants, heating temperature at 200^{o}C and 290^{o}C, and the sustained heating time on the particle size distribution and composition

are discussed.

4.1.1 Size control of FePt nanoparticles

Seed-mediated growth method

The synthesis of FePt nanoparticles were carried out by using commercially available reagents without further purification. The synthesis steps are as following: platinum acetylacetonate (0.25 mmol), 1,2-hexadecanediol (1 mmol), dibenzyl ether (10 mL), and oleic acid (0.5 mmol) were mixed in three neck- round bottom flask and heated to 110^{o}C. Oleyl amine (0.5 mmol) and pentaccarboyl iron ($Fe(CO)_5$) (0.75 mmol) were added sequently and then the mixture was heated and reflux at 290℃ for 30 minutes. The heating rate was kept at 5^{o}C/min. The heat source was then removed and the reaction mixture was allowed to cool to room temperature. The black products was precipitated by adding 20 mL ethanol and collected by centrifugation with 5000 rpm for 5 min. The 2.7 nm FePt seeds were obtained and re-dissolved in hexane with the presence of 20 μL oleic acid and 20uL oleyl amine. 3 nm FePt nanoparticles were obtained via the same synthetic procedure with 2.7 nm FePt nanoparticles as seeds. 2.7 nm FePt seeds were mixed with platinum acetylacetonate (0.25 mmol), 1,2-hexadecanediol (1 mmol) , dibenzyl ether (10 mL) and oleic acid (0.5 mmol). The mixture was heated to 110^{o}C and followed by injection of oleyl amine (0.5 mmol) and $Fe(CO)_5$

(0.75 mmol). 2.9 nm FePt were obtained after the mixture reflux at 290°C for 30 min. 4.4 nm FePt nanoparticles were synthesized with the 3 nm FePt as seeds at the same reaction conditions. By using seed-mediated growth, bigger FePt nanoparticles have been made.

The TEM images shown in the Figure 4.1 indicate that the serial seed-mediated growth effectively tune the size of FePt nanoparticles and the mean diameter slightly increase from 2.67±0.51 to 3.67±0.70 nm. However, the size distribution is broad. The size distribution is shown on the right of each TEM image.

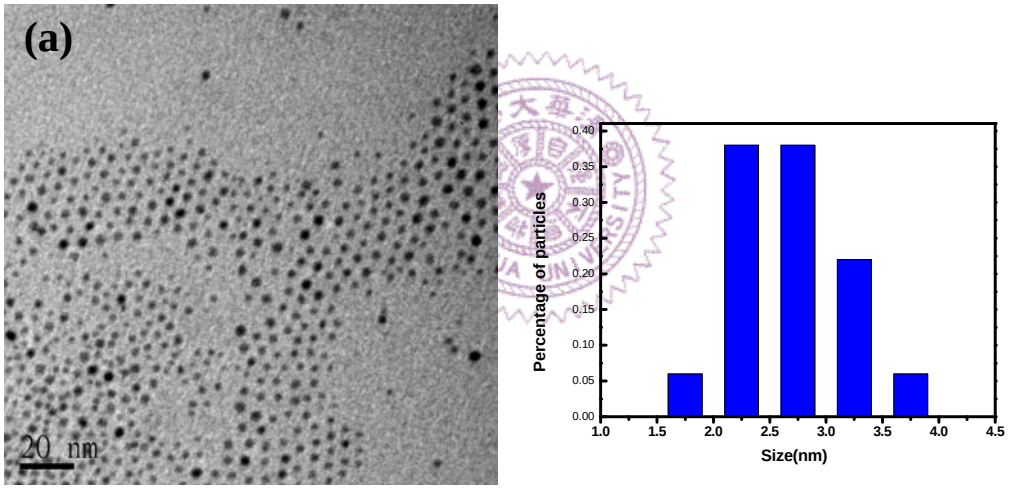

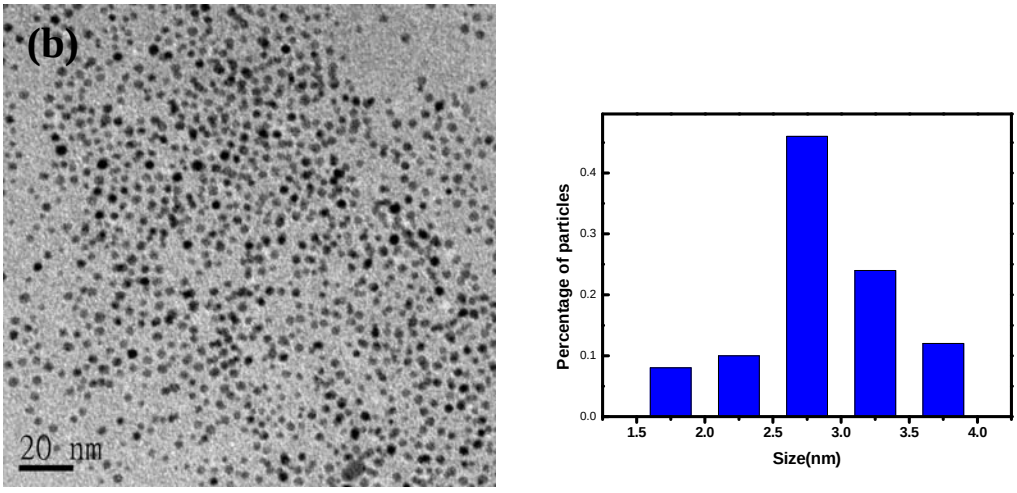

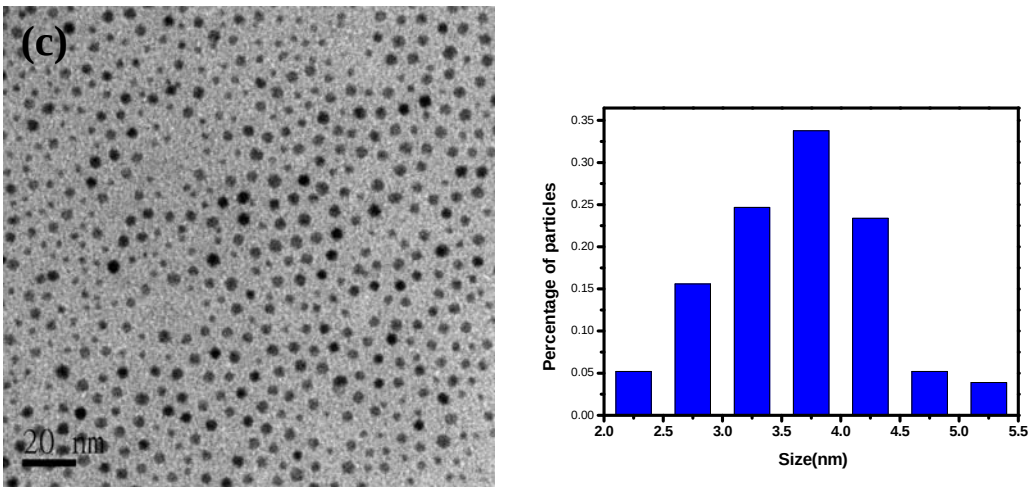

Figure 4.1 *The TEM images of FePt nanoparticles were synthesized by seed-mediated process. (a)2.67 nm. (b) 2.86 nm. (c) 3.67 nm*

Seed mediated growth always includes two stages of nucleation and growth. So called homogeneous nucleation should be the reaction without extra seed. When the extra seeds were added, they play the role of seeds which monomers grow on. Meanwhile, the homogeneous nucleation still happens. The seed from homogeneous nucleation is like a cluster which has very high surface energy. Parts of seed cluster will re-dissolve in solution and then grow on the surface of larger particles which are lower surface energy. This process is called “Ostwarld Ripen”. In this method, the seed- nanoparticles are introduced into the solution and then the monomers are supplied to precipitate on the surface of the existing nuclei. The monomer is kept at low concentration during growth to suppress homogeneous nucleation. Hence, suppressing the homogeneous nucleation during series seed-mediated growth is the key to narrowing the

size distribution. For the three times of seed-mediated processes, the size distributions are broad (shown in Figure 4.1(c)).

The different concentration of the surfactants

Surfactants typically play a crucial role in controlling the size and shape of chemically synthesized nanoparticles. Oleic acid and oleyl amine were chosen in my synthesis as they work as ideal ligands for FePt nanoparticles. The effect of surfactants to $Pt(acac)_2$ molar ratio on the size of FePt nanoparticles were shown in figure 4.2 and 4.3. By decreasing the molar ratio to 2, the particle size decreased to 3.46 nm (Figure 4.2(a)) while by increasing the molar ratio up to 12, the particle size increased to 5.12 nm (Figure 4.2(e)). It is seen that the particle size increase with increasing surfactant concentration (Figure 4.3).

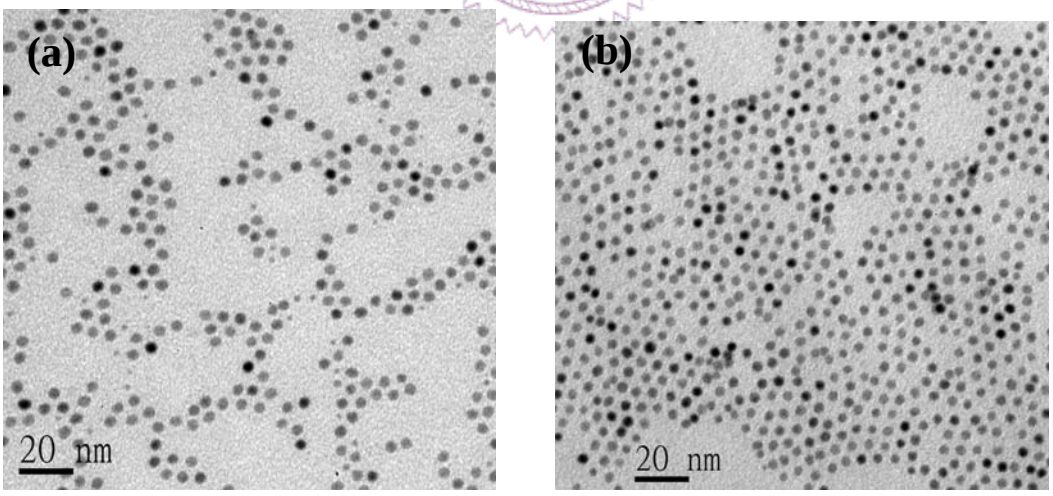

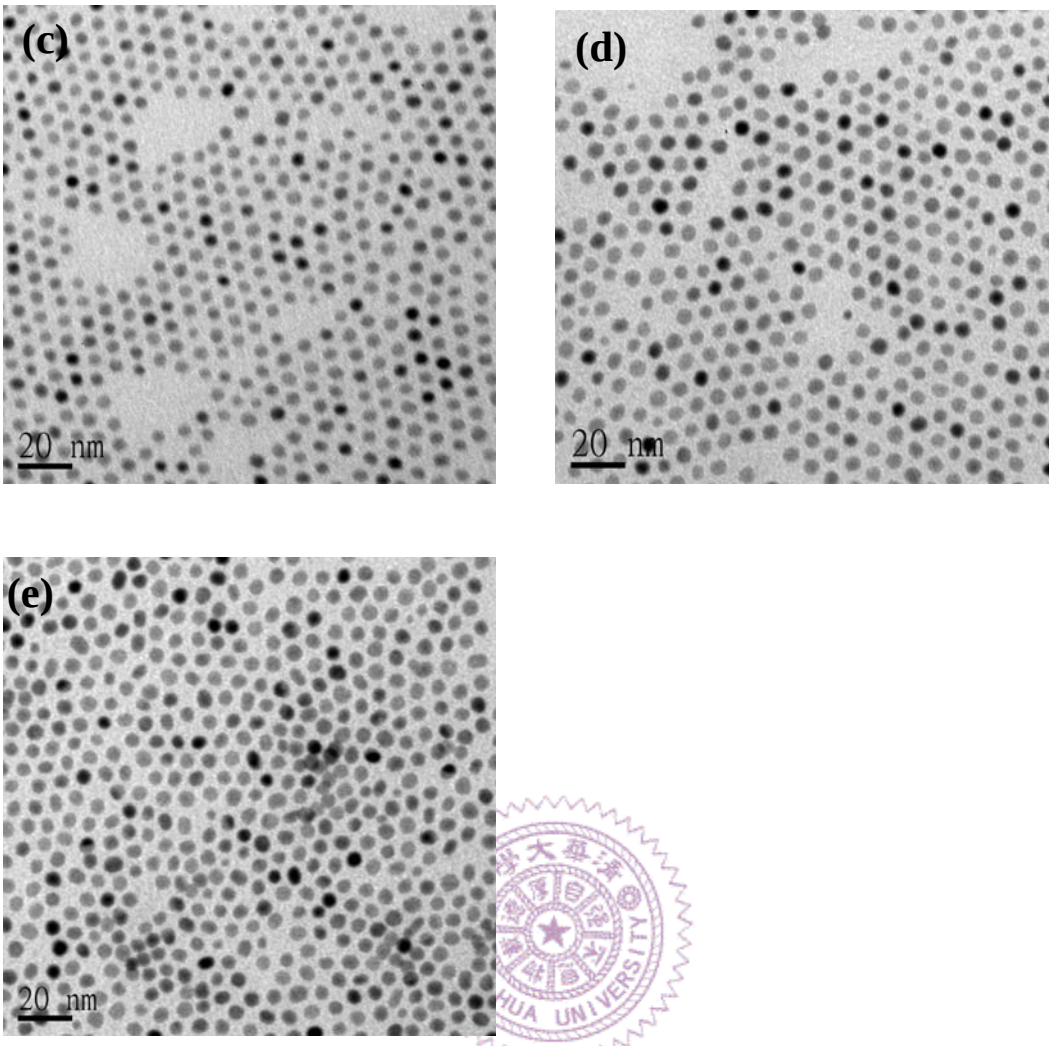

Figure 4.2 *TEM images of as-synthesized FePt nanoparticles with different molar ratio of surfactant / $Pt(acac)_2$. (a)ratio= 2 , 3.46±0.35nm, (b) ratio=5, 3.30±0.29 nm, (c) ratio=8, 4.11±0.38nm,(d) ratio=10, 4.94±0.44nm,and(e)ratio=12,5.12±0.44nm*

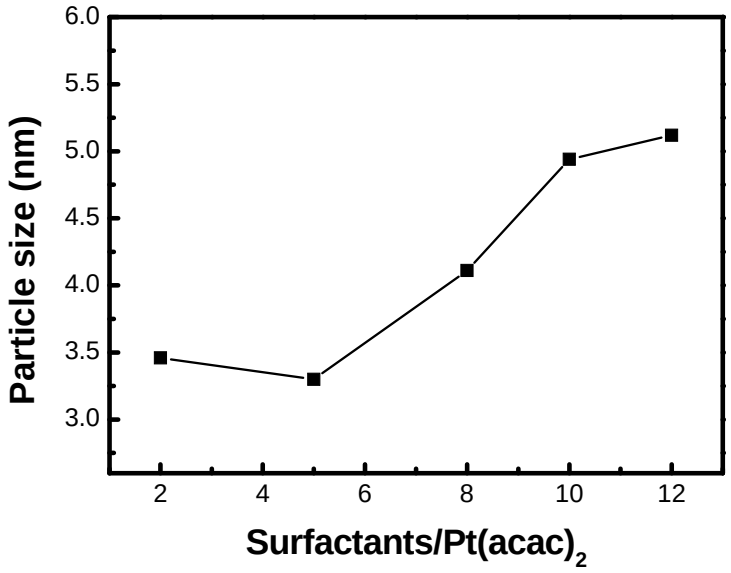

Figure 4.3 *particle size dependence on the surfactants/Pt(acac)$_2$*

The influence of surfactant concentration on the particle size is related to growth kinetics of nanoparticles. This phenomenon had been found by Nandwana Elkins *et al.* in years [22]. The influence on the CdS and other semiconductor nanocrystals also has been reported[54]. There is a possibility that the reactivity of platinum monomers increases with decreasing the surfactants concentration. It helps the nucleation rate of platinum, so the average size of nuclei decreases. On the contrary, the increase in the surfactant amount resulted in the formation of stable complexes with individual metal atoms of a molecular precursor. Therefore, an increase in surfactant concentration is expected to suppress the nucleation process and as a consequence, larger particle size is produced.

The different heating time

In order to study the relation between the heating time with different amount of surfactants and particle size, the ratio of the surfactants to platinum was taken as 2 and 20, and the heating time of 290^{o}C was varied from 0.5h to 2h. For the molar ratio of 20, the average size for 0.5h and 2h refluxed particles were 4.97 and 7 nm; for the molar ratio of 2, the size for 0.5h and 2h refluxed particles were 3.97 and 4.48 nm. It is an evident that the particle size increases with increasing heating time. The relation between the particle size and the heating time is shown in Figure 4.4.

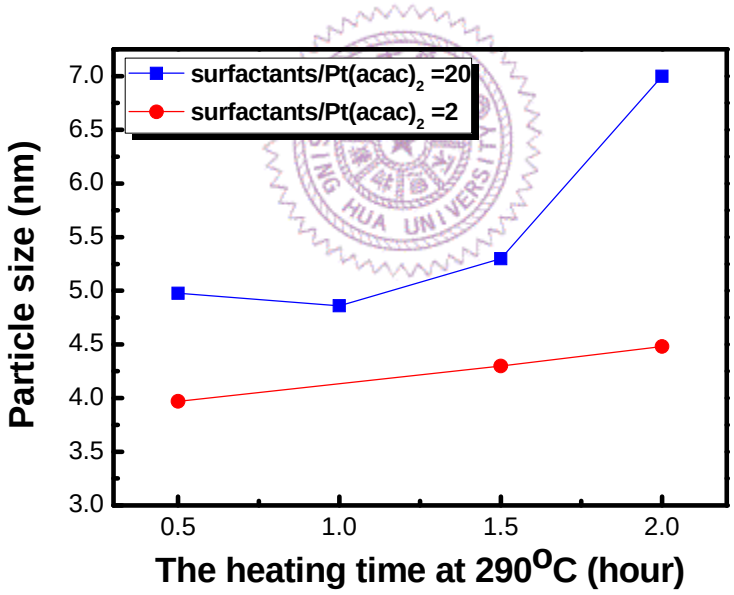

Figure 4.4 *Particle size versus the heating time of 290^{o}C at different concentrations of the surfactants*

When the concentration of surfactants is high, the increment in particle size is significant. Besides, the particle sizes for the molar ratio of

20 are larger than these for the molar ratio of 2.

Separation of nucleation and growth makes it possible to control the particle size and size distribution. According to the previous reports[48], two heating stages were adopted. A low temperature of 200 °C provides the nucleation for iron oxide, and then a higher temperature of 290 °C provides the growth. It is known that Pt nuclei formed initially at 160°C and $Fe(CO)_5$ starts to decompose at 175 °C. The additional reaction temperature of 200°C is expected to decrease the nucleation rate and larger particles can be obtained. To study the effect of the reaction temperature of 200°C on the particle size, the heating time of 200°C is varied from 0.5h to 2h.

The synthetic process is given below. 0.25 mmol of $Pt(acac)_2$,1 mmol of 1,2-hexadecanediol, 0.5 mmol of oleic acid were mixed with 10 mL dibenzyl ether. Argon atmosphere were maintained during the synthesis. The reaction mixture was heated to 110°C, and at this temperature 0.75 mmol of $Fe(CO)_5$ and 0.5 mmol of oleyl amine were injected. The temperature was then raised to 200 °C for various periods of time. The temperature was then raised to 290°C for 0.5h.

Figure 4.5 shows the relation between the particle size and the heating time of 200 °C for various concentrations of the surfactants. It is clearly seen that the particle size increases with increasing the heating time. However, further increasing the heating time to 4h, the particle size did not increase. Therefore, there is a limitation on the increased particle size through increasing the heating time of 200 °C.

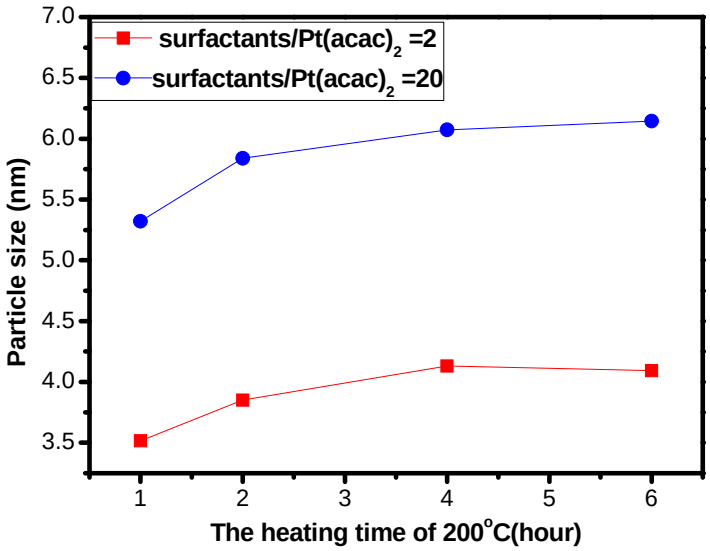

Figure 4.5 *Particle size versus the heating time of 200°C at different concentrations of the surfactant*

4.1.2 Composition control over FePt nanoparticles

The composition of FePt nanoparticles is controlled by manipulating the concentration of the surfactants and the heating time. Although larger particle size could be produced via series seed-mediated processes described in the previous section, the control of the composition on Fe/Pt ratio becomes difficult. The XRD patterns of annealed FePt nanoparticles (figure 4.6) show the different crystalline structure of as-synthesized FePt nanoparticles. When the number of times of seed-mediated process increased, the position of (111) peak shifts to the low angle. It is indicated

that $L1_2$ $FePt_3$ phase appears. The relation between the XRD pattern and the structure will be discussed more detailed in the following section. The amount of Fe in the FePt nanoparticles decreases with increasing the times of seed-mediated process. It may attribute to that the excess surfactants around the Fe atoms would obstruct Fe atoms incorporating in the FePt nanoparticles. The excess of surfactants on the surface of the seed-FePt may hinder Fe atom from diffusing into seed-FePt nanoparticles, so it forms platinum-rich Fe-Pt alloy.

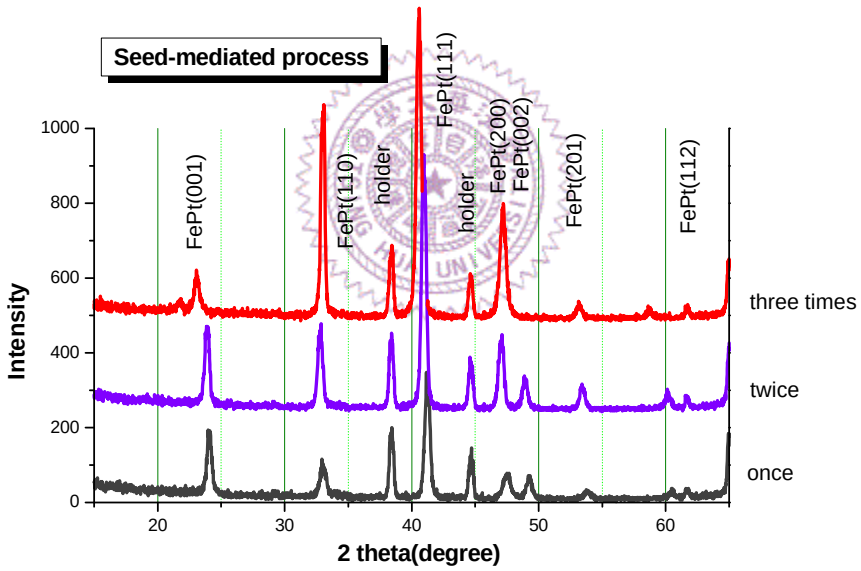

Figure 4.6 *XRD patterns of the annealed FePt nanoparticles*

The concentrations of the surfactants control not only the size of FePt nanoparticles but also the composition of them. In order to study the effect of surfactants on the composition, the surfactants to $Pt(acac)_2$ molar ratio was varied while keeping all the synthetic conditions the same. It was observed that increasing the molar ratio resulted in the decreasing of

Fe atoms in the FePt nanoparticles. It is due to that the Fe could form metal-organic complexes with the surfactants, so the larger amount of oleic acid can stabilize the Fe atoms. The supersaturation of the Fe species produces the Fe rich cluster during the initial stage of synthesis and do not diffuse into Pt clusters[55]. Besides, formation of Fe^{o} dose not correspond to the formation of FePt alloy nanocrystals. This is because the pure iron phase is also a stable phase.

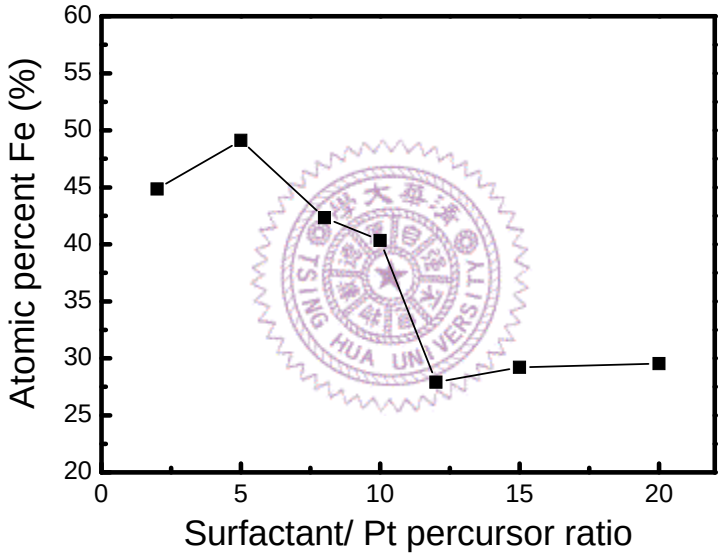

Figure 4.7 *Variations in atomic percent of Fe with the surfactants/Pt precursor for the 30 min reflux*

To study the evolution of the composition change in FePt nanoparticles, small amount of the reaction mixture was withdrawn at 290^{o}C with various heating time. The relation between Fe content and the heating time is shown in Figure 4.8.

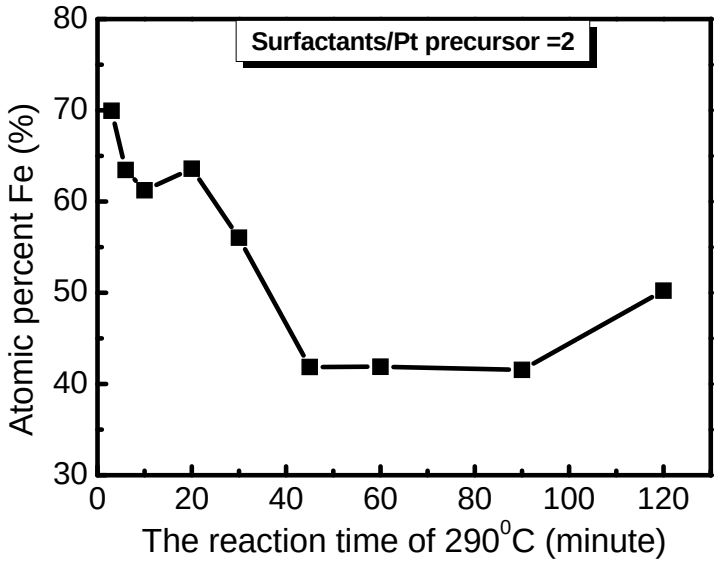

Figure 4.8 *Compositional evolutions of FePt nanoparticles at various heating time*

At the beginning, the Fe content is more than Pt. The possible reason has been demonstrated by the heterogeneous synthesis [56, 57]. Platinum nuclei were formed by the reduction of $Pt(acac)_2$. During the early stage of synthesis, Fe or FeO_x coat Pt seeds and Pt can catalyze FeO_x to Fe. Diffusion of Fe atom takes place when the temperature reaches the boiling point of benzyl ether. The possible schematic mechanism is illustrated in Figure 4.9.

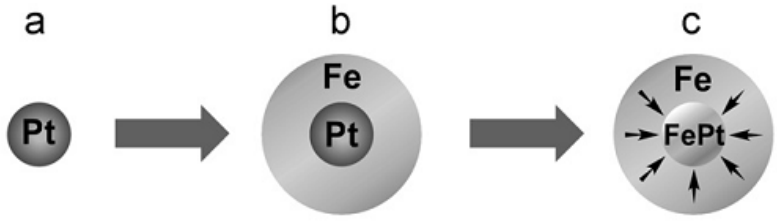

Figure 4.9 *Schematic illustration of the heterogeneous synthesis of FePt nanoparticles. Formation of Pt seeds (a), nucleation and growth of Fe during first stage (b), diffusion of Fe in the core at high temperature [56].*

Figure 4.10 shows the morphology of FePt nanoparticles at various heating time of 290 °C. When the FePt nanoparticles are withdrawn at 3 min reflux, the shell-like substance appears around the surface of each particle. It corresponds to Figure 4.10(b). The possible structure is iron or iron oxide. Further increasing the reflux time, the iron diffuses into Pt-rich nuclei and the shells disappear. The size of final particle is about 3nm.

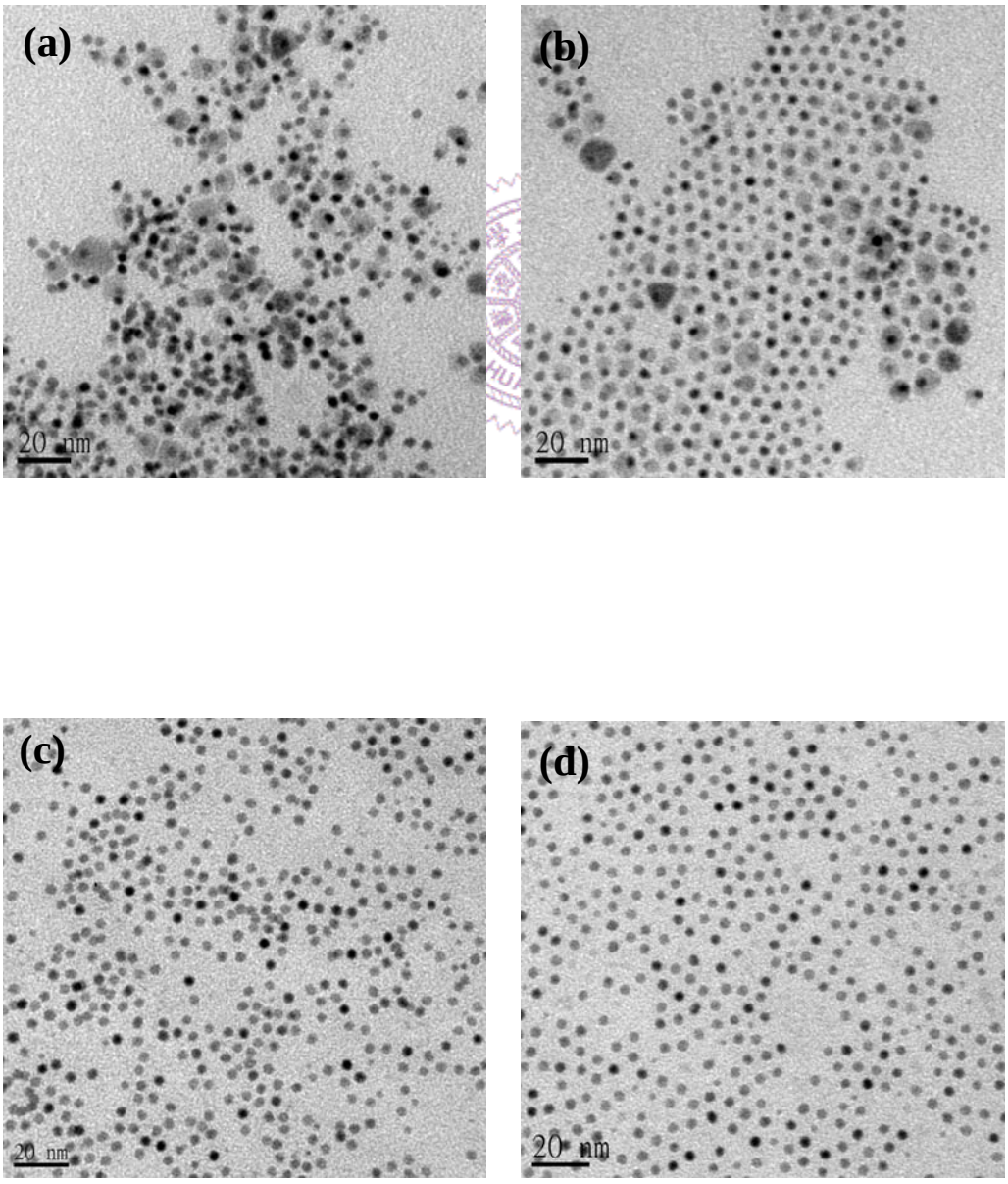

Figure 4.10 *TEM images of FePt nanoparticles withdrawn at (a) 3 min reflux, (b)10 min reflux,(c)60 min reflux, and (d) 120 min reflux*

Further prolong the heating time, the Fe content decreases. It is because that parts of $Fe(CO)_5$ vapor lose by the Ar flow. As the reflux time increased, the ratio of Pt content to Fe content increased

4.2 Magnetic properties of annealed FePt nanoparticles

4.2.1 Phase transformation of FePt nanoparticles

In the phase diagram, the stability of bimetal materials is dependent on the composition and temperature[58] . Below 1600K, the bulk FePt alloy undergoes a phase transition from a face-centered-cubic-base (fcc) solid solution into a ordered face-centered tetragonal (fct, $L1_0$) phase[59]. The fcc-structured FePt has a small coercivity and is magnetically soft. The fully ordered fct-structured FePt possess high anisotropy(K ~$10^7 Jm^{-3}$) along the easy axix. Hence, post-annealing is necessary for the formation of FePt nanoparticles with fct structure. In my experiment, FePt nanoparticles are annealed at temperature of 800 ℃ for 1h under the forming gas(10%H_2 +90% Ar).

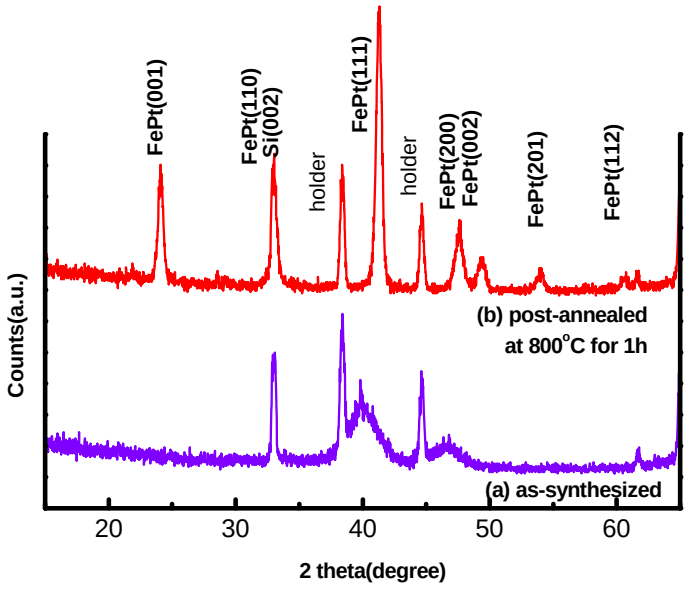

Figure 4.11 *XRD patterns of the as-synthesized and annealed FePt nanoparticles*

Figure 4.11 shows the XRD pattern of the FePt nanoparticles before and after annealing. From the XRD patterns, we can find that the 2θ of (111) peak shifted to the high angle after annealing. Moreover, the appearance of (001) and (110) peaks means the phase transition of FePt from fcc to fct structure. The fully ordered fct-structured FePt can be viewed as alternating atomic layer of Fe and Pt stacked along the [001] direction. Such a structure gives rise to the appearance of the forbidden peaks of (001) and (110). Figure 4.12 schematically illustrates the fct-structured FePt. The difference of the hysteresis loop before and after annealing is shown on Figure 4.13. The large coercivity is up to 8000 Oe, indicating the fct-structured FePt could be obtained.

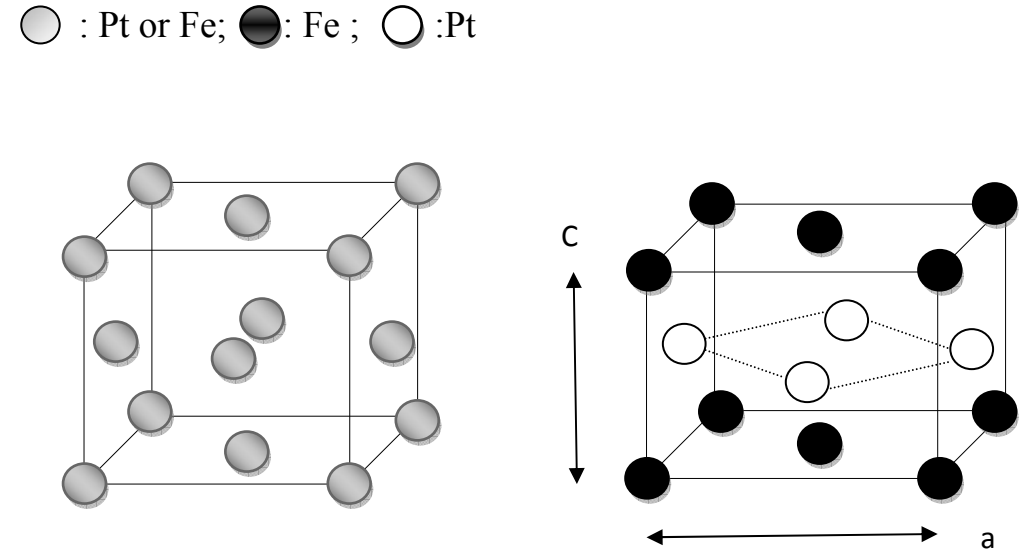

(A) A1 phase (disorder fcc)

a: 3.816Å

(B) $L1_0$ phase (order fct)

a: 3.853Å, c: 3.713Å

Figure 4.12 *Schematic illustration of the unit cell of A)chemically disordered fcc and B) chemically ordered fct*

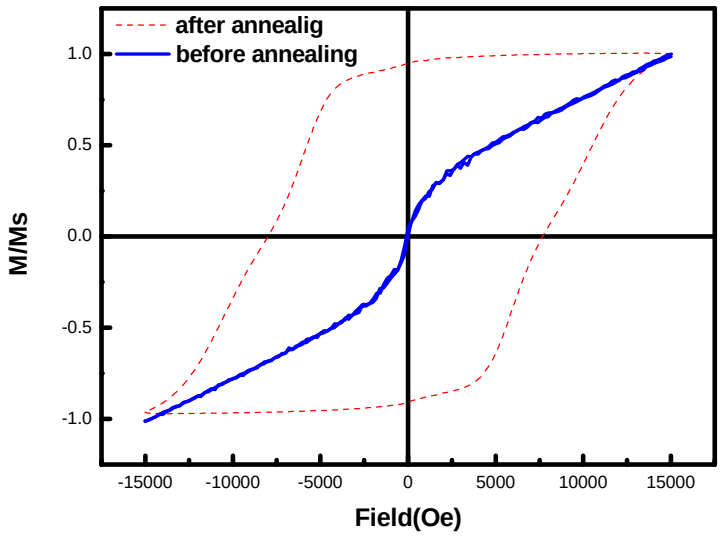

Figure 4.13 *Hysteresis loop of FePt nanoparticles before and after annealing*

4.2.2 Magnetic properties of FePt and $FePt_3$ nanoparticles

The composition of FePt is very sensitive to the synthetic parameters. The FePt and $FePt_3$ can be obtained by adjusting the concentration of the surfactants and the heating time (section 4.1). The magnetic properties of FePt strongly depend on the composition. Slight difference in composition leads to obvious difference in magnetism. Fe_xPt_{1-x} with X=40~68 posses the maxima coercivity[18] and will be a candidate for ultra-high density magnetic recording materials.

Figure 4.14 shows the hysteresis loop of FePt nanoparticles annealed at 800℃ under the forming gas. The synthetic parameters are as following: $Pt(acac)_2$(0.25 mmol), 1,2-hexadecanediol (1 mmol), dibenzyl ether (10 mL), and oleic acid (2.5 mmol) were mixed in three neck- round bottom flask and heated to 110°C. Oleyl amine (2.5 mmol) and ($Fe(CO)_5$) (0.75 mmol) were added sequently and then the mixture was heated and reflux at 290℃ for 30 minutes. The heating rate was kept at 5°C/min. The large coercivity of 1T Oe means that as-synthesized FePt nanoparticles are fully ordered.

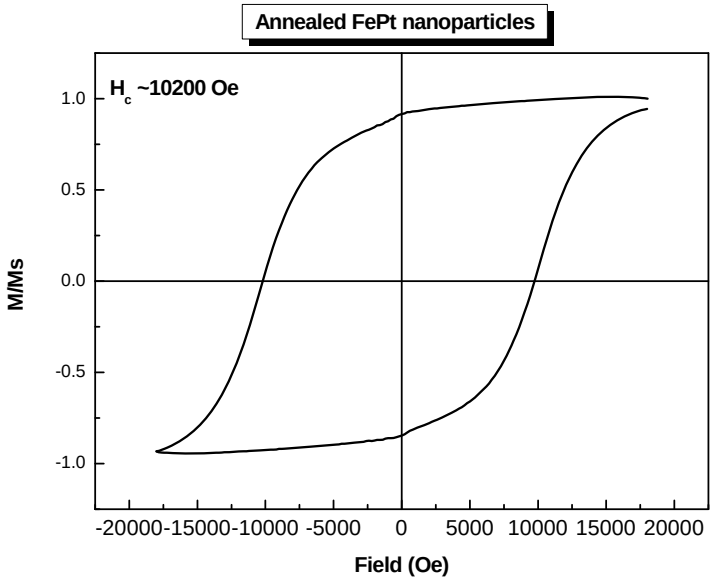

Figure 4.14 *Hysteresis loop of annealed FePt nanoparticles.*

Figure 4.15 shows the hysteresis loop of $FePt_3$ nanoparticles annealed at 800℃ under the forming gas. It is clearly seen that the shapes of hysteresis loops for $FePt_3$ is very different from FePt. Chemically ordered fct structure of FePt is ferromagnetism (FM) while chemically ordered fcc structure of $FePt_3(L1_2)$ is antiferromagnetism(AFM).

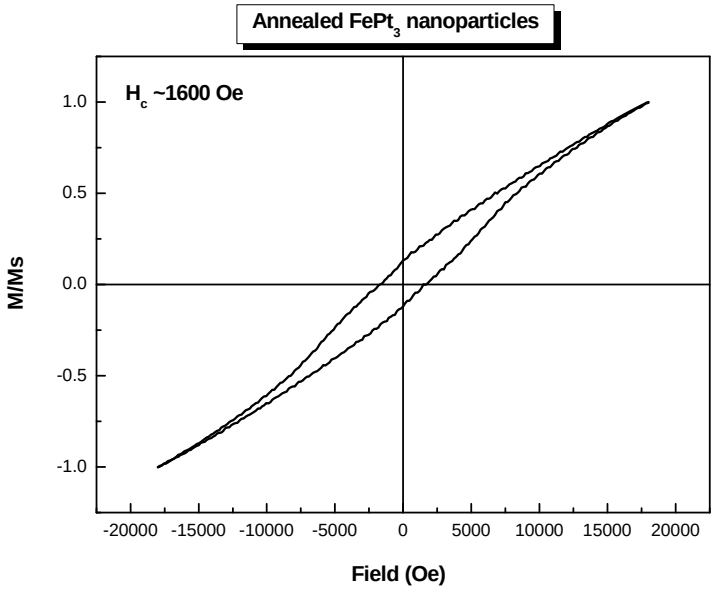

Figure 4.15 *Hysteresis loop of annealed $FePt_3$ nanoparticles.*

The physics of $FePt_3$ is interesting. The chemically disordered phase is ferromagnetic while the chemically ordered phase is antiferromagnetic. The $FePt_3$ with chemically ordered phase exhibit two different type of AF order as depicted in Figure 4.16. In bulk, the appearance of these two AF phase depends strongly on the variation of composition. The $FePt_3$ phase is maintained in Fe_xPt_{1-x} alloys with $0.22<X<0.41$. Upon cooling, bulk $FePt_3$ develops AF order below T_{N1}=160K, where the magnetic moments of Fe order in alternating ferromagnetic sheets in the (110) planes. For slightly Fe-rich alloys, the phase is ordered in alternating ferromagnetic sheets in the (100) planes[60].

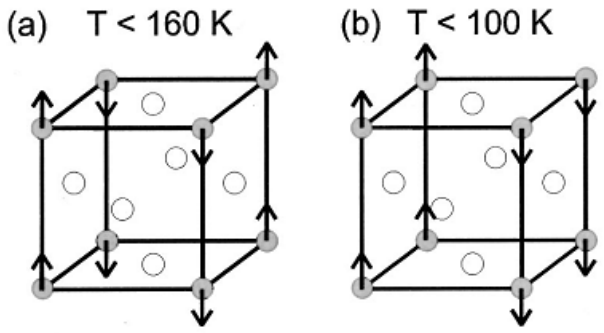

Figure 4.16 *The different types of AF for $FePt_3$. The grey spheres represent the Fe atoms, which form a simple cubic lattice, and the white spheres represent Pt atoms[60].*

XRD patterns were shown in figure 4.17 and show some difference owing to the different structure in FePt and $FePt_3$. The peak position of

(111) shift to low angle because the lattice constant of $FePt_3$ (a=3.87Å) is larger than that of FePt (a=3.853Å, c=3.713Å). Besides, the appearance of (002) peak in the XRD pattern of FePt was found. The original (200) peak splits into (200) and (002) because the lattice constants of *c* and *a* are different for fully ordered FePt.

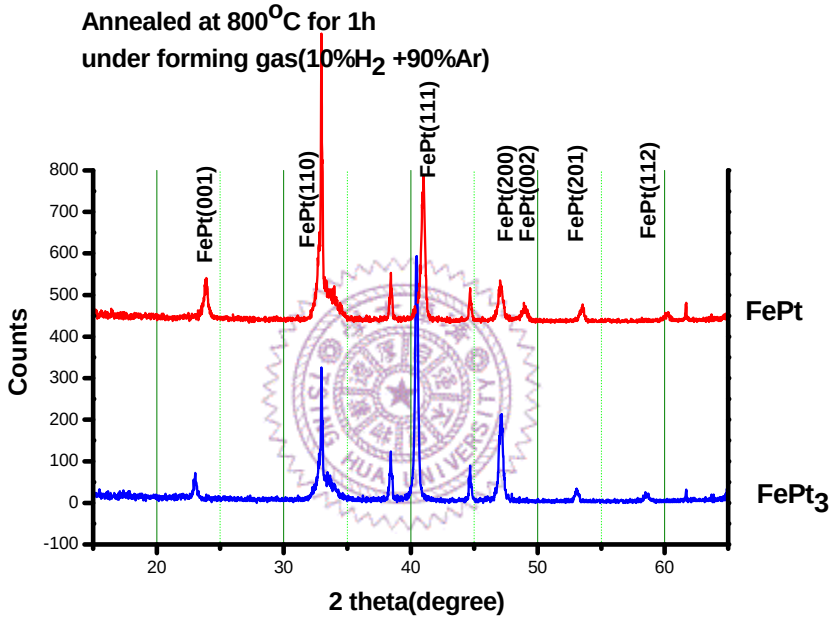

Figure 4.17 *The XRD patterns of annealed FePt and $FePt_3$ nanoparticles.*

4.2.3 FePt nanoparticles annealed in salt matrix

How to avoid sintering and aggregation of FePt nanoparticles in annealing process is a big issue. A lot of efforts on the issue have been reported: rapid thermal annealing[61], pulse laser annealing[36], and

salt-matrix annealing [33]. Herein, we choose salt-matrix annealing to obtain fct FePt nanoparticles owing to its easy handling and cheap.

Figure 4.18 shows the as-synthesized FePt nanoparticles with different size (from 3 to 8 nm) annealed in salt matrix. For the FePt particles with 3nm and 4.5 nm, the size and shape are retained after annealing. However, for the FePt particles with 5.5nm and 8 nm, some large particles as big as 20 nm are observed.

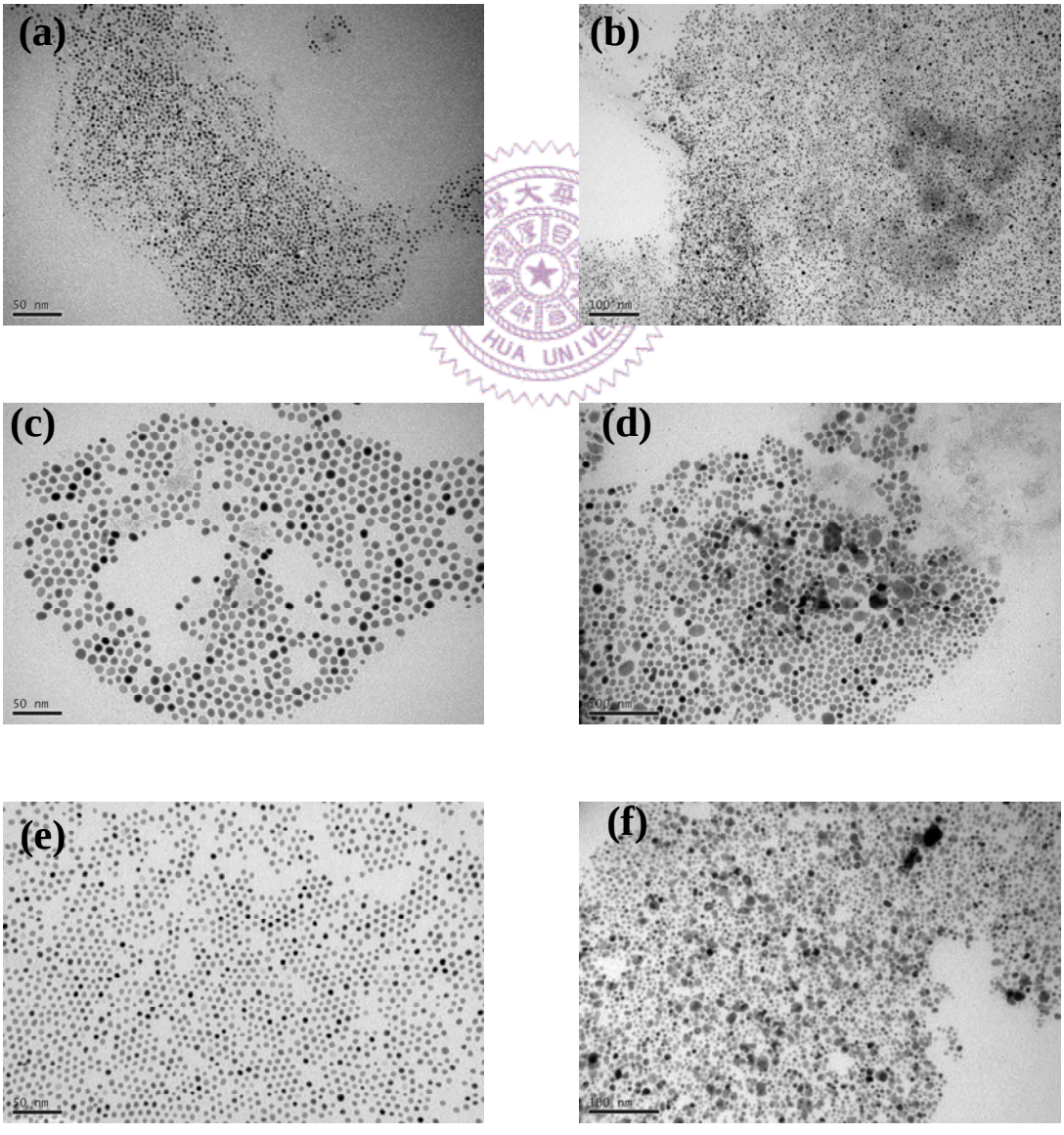

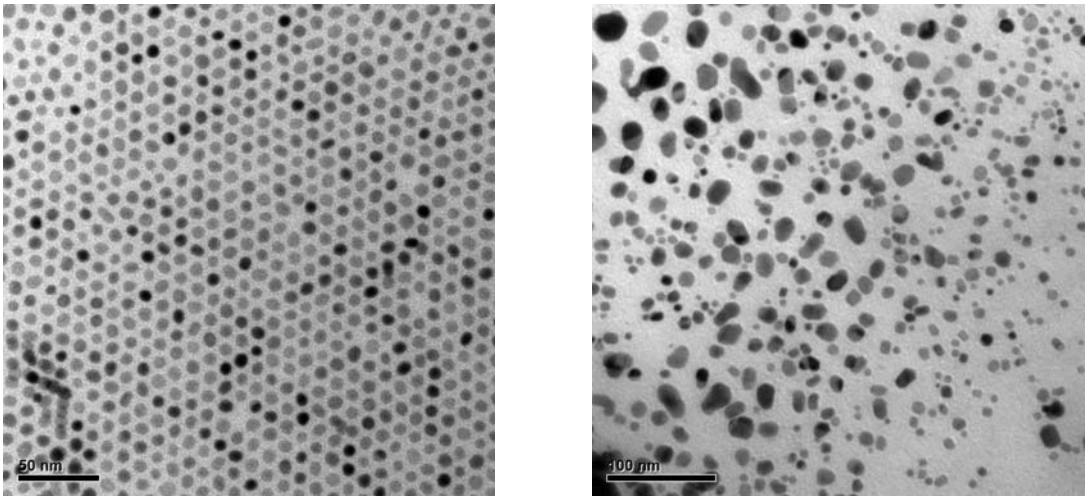

Figure 4.18 *TEM images of the as-synthesized FePt with different sizes, (a) 2.9nm, (c) 5.35nm, (e)4.6nm, and (g) 7.9nm are nanoparticles. Images of (b), (d), (f), and (h) are FePt particles annealed in salt matrix at 800℃ for 1h ,corresponding to each of the left image ,respectively*

Besides, the size distribution became wide after annealing. The appearance of large particles means that sintering occurred during annealing. It was reported that the NaCl-to-FePt ratio is an important factor for sintering. If the amount of salt is large enough, each FePt nanoparticle is surrounded by salt. In this way, sintering can be avoided during annealing.

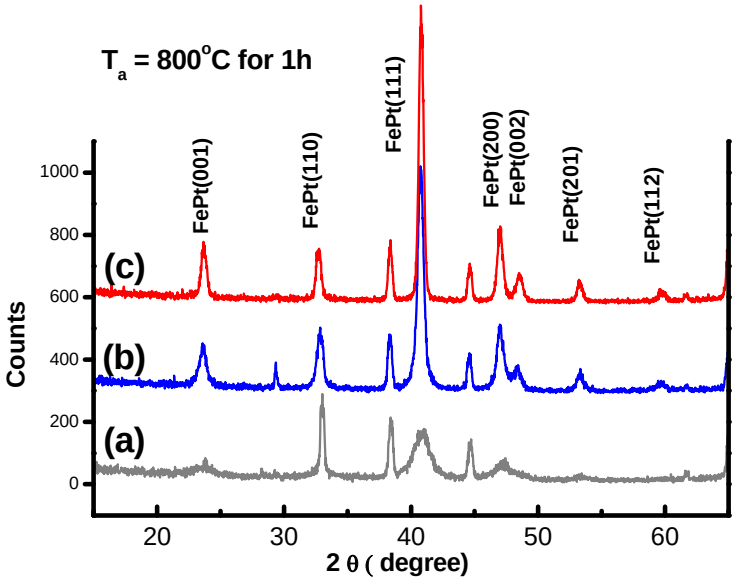

Figure 4.19 *XRD patterns of (a) 2.9nm, (b) 4.6nm, and (c) 5.35nm FePt nanoparticles annealed at 800℃ for 1h*

Figure 4.19 shows the XRD pattern of the FePt nanoparticles with different sizes annealed in salt matrix. It was found that superlattiec peak of (001) and (110) appear, indicating the formation of an ordered $L1_0$ γ_2-FePt phase. For the FePt nanoparticles with 3 nm, the (111) peak is broad. It indicated that the size is retained and the sintering did not appear.

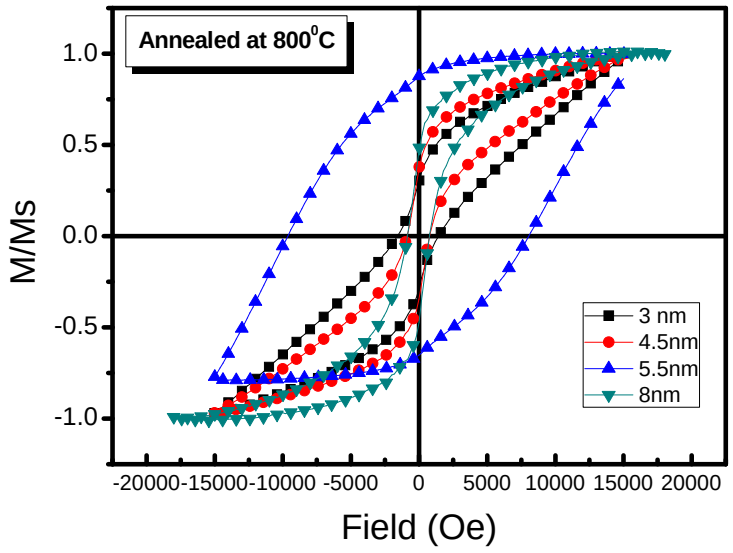

Figure 4.20 *Hysteresis loops of 3, 4.5 , 5.5, and 8 nm FePt nanoparticles annealed at 800℃ for 1h.*

Experimental and theoretical studies have shown that the degree of chemical ordering in FePt nanoparticles is related to the particle size . Ordering cannot be achieved when the particle size is below a critical size. In the case of 3nm FePt nanoparticles, the coercivity is about 1600Oe. The loop show some kinks at Hc ~0, indicating partial chemical ordering due to the particle size or atomic composition during the particle size.

4.3 Nanocomposite of FePt and $FePt_3$

Exchange-spring magnets are composed of magnetically hard- and

soft- grains that have potential application as permanent magnets. The hard-magnetic grains provide the high anisotropy and coercivity fields while the soft-magnetic grains enhance the magnetic moments. Here we report the fabrication of the exchange-coupled nanocomposite using nanoparticles self-assembly.

4.3.1 Magnetic properties of the mixture of FePt and $FePt_3$

$Fe_{40}Pt_{60}$ and $Fe_{29}Pt_{71}$ nanoparticles are fabricated according to the previous experiments. The size of $Fe_{40}Pt_{60}$ is 4.94±0.44nm and $Fe_{29}Pt_{71}$ is 3.7±0.0.37nm.

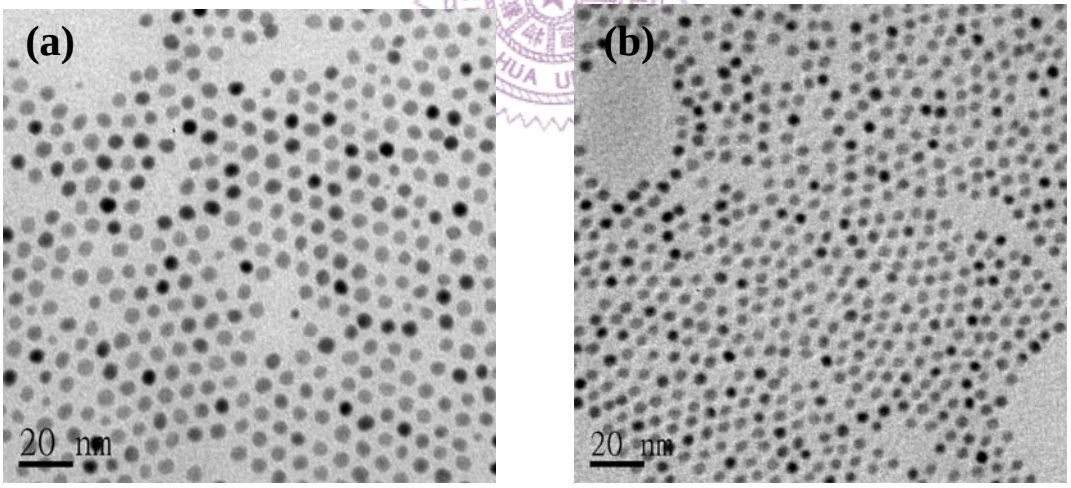

Figure 4.21 *TEM images of (a) 4.94±0.44nm $Fe_{40}Pt_{60}$, and (c) 3.7±0.37nm $Fe_{29}Pt_{71}$*

Hexane dispersion of $Fe_{40}Pt_{60}$ and $Fe_{29}Pt_{71}$nanoparticles with selected size was mixture under ultrasonic agitation. The mass ratio of $Fe_{40}Pt_{60}$ and $Fe_{29}Pt_{71}$ was controlled in the rage of 1:1. The binary nanoparticles

were converted into FePt-$FePt_3$ nanocomposite by post-annealing under forming gas (10%H_2 +90%Ar) at 800°C for 1h. The annealing transforms the FePt from disordered f.c.c. to ordered f.c.t structure. $FePt_3$ is also transforms from disordered f.c.c. to ordered f.c.t. structure. The high temperature annealing can desorbs the surfactants around each nanoparticle, allowing the nanoparticles sintering.

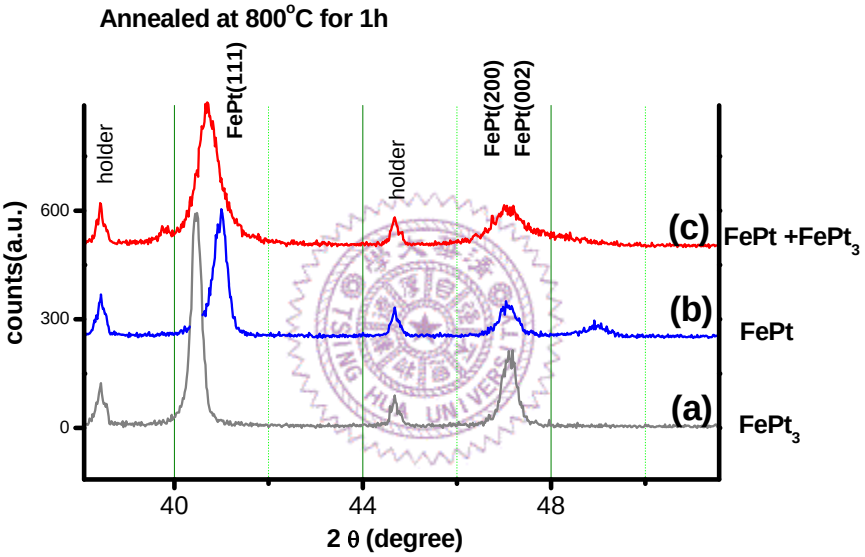

Figure 4.22 *XRD patterns of (a) annealed FePt, (b) annealed $FePt_3$, and (c) annealed the mixture of FePt and $FePt_3$*

From the XRD patterns (shown in Figure 4.22), it is clearly seen that the position of (111) peak is just between the (111) peak of FePt and the (111) peak of $FePt_3$. It implied that the two nanoparticles were well mixed.

Figure 4.23 is the hysteresis loop for the composite from the FePt and $FePt_3$ with 1:1 mass ratio. The hysteresis loop shows that the

magnetization changes smoothly, like a single-phase material. It can be inferred that the exchange coupling between two phases exists[62].

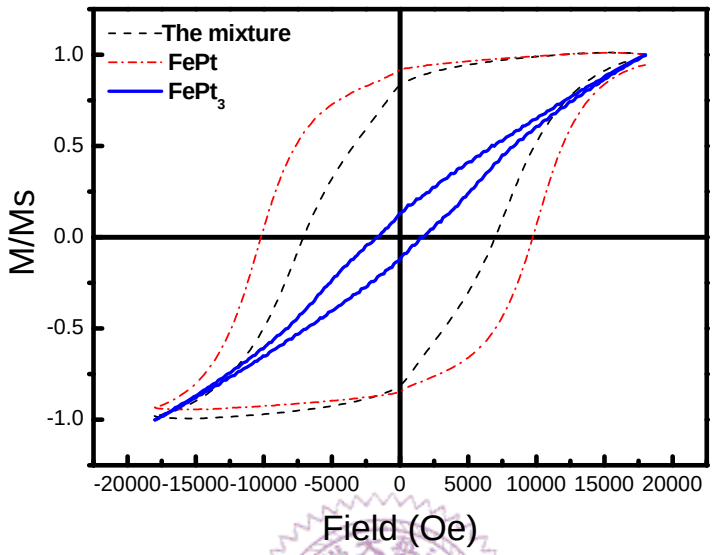

Figure 4.23 *The hysteresis loop of the nanocomposite. The composite was made from the annealed FePt and $FePt_3$ assemblies with mass ratio being kept at FePt: $FePt_3$=1:1*

4.3.2 The mixture of FePt and $FePt_3$ annealed in salt matrix

Compared with the FePt-$FePt_3$ as a thin film, we want to investigate the FePt-$FePt_3$ nanocomposite as a nanoparticle. It is to say, we want to fabricate the isolated FePt-FeP_3 nanoparticles. To prevent the particles from sintering, the salt-matrix annealing has been adopted. Hexane dispersions of FePt and $FePt_3$ nanoparticles were well mixed under

ultrasonic agitation. The mass ratio was controlled in the range of 1:1. Then the salt powders were mixed with the mixture, and weight ratio of the salts to the mixture was varied. The mixtures were annealed at temperature of 800^{o}C for 1h under forming gas (10%H_2 + 90%Ar). After annealing, the salt was removed from the samples by washing the mixtures in deionized water.

Figure 4.24 shows the hysteresis loop of annealed FePt-$FePt_3$ nanocomposite. The magnetization linearly depends on the field when the ratio of NaCl to FePt-$FePt_3$ is 100. The phenomenon can be ascribed to the exchange spring. It was known that the bulk $FePt_3$ is antiferro-magnetic. However, $FePt_3$ also shows the ferromagnetic behavior when the size decreases to the critical value. It was attributed to the uncompensated surface spins originating from the finite size effect. Because of the uncompensated surface spins, the $FePt_3$ nanoparticles possess soft-ferromagnetic behavior[63]. The exchange spring comes from the magnetically hard FePt nanoparticle and magnetically soft $FePt_3$ nanoparticles. From the TEM image, shown in Figure 4.25, the isolated FePt-$FePt_3$ nanoparticles can be obtained.

The diffraction peaks of FePt and $FePt_3$ are similar, so it is difficult to tell $FePt_3$ from FePt. However, around $2\theta=23^{o}$, there are two peaks. It is suggested that FePt and $FePt_3$ coexist, shown in Figure 4.26.

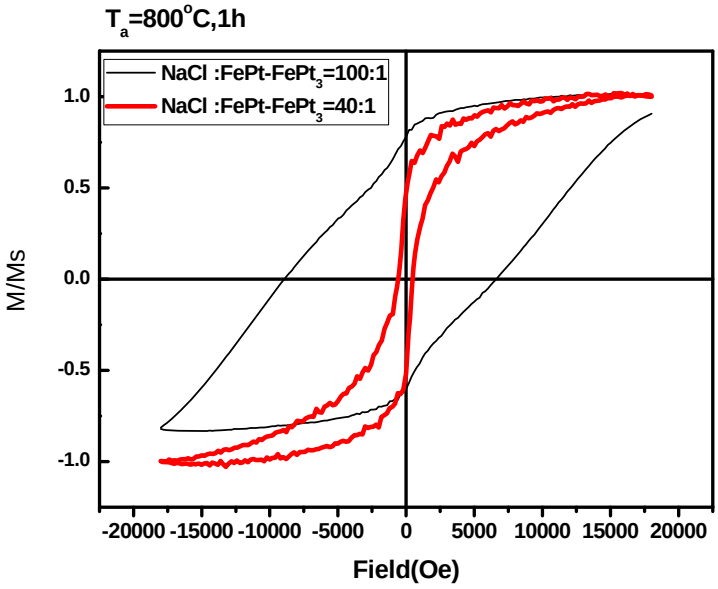

Figure 4.24 *The hysteresis loop of annealed FePt-FePt$_3$ with the different ratio of the salt to FePt-FePt$_3$*

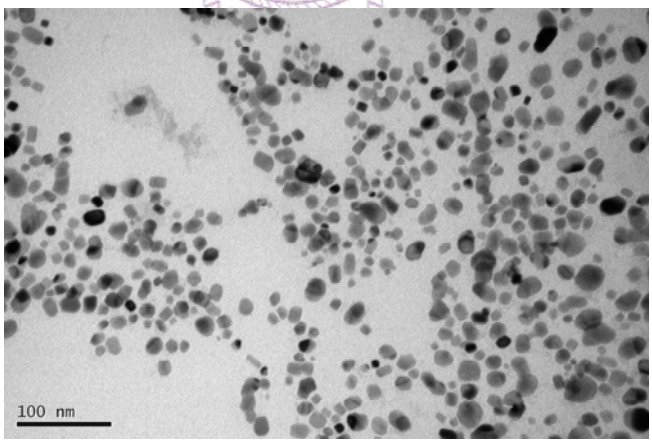

Figure 4.25 *TEM image of FePt-FePt$_3$ nanocomposite annealed in NaCl matrix at 800°C for 1h with NaCl-to-FePt ratio of 100:1*

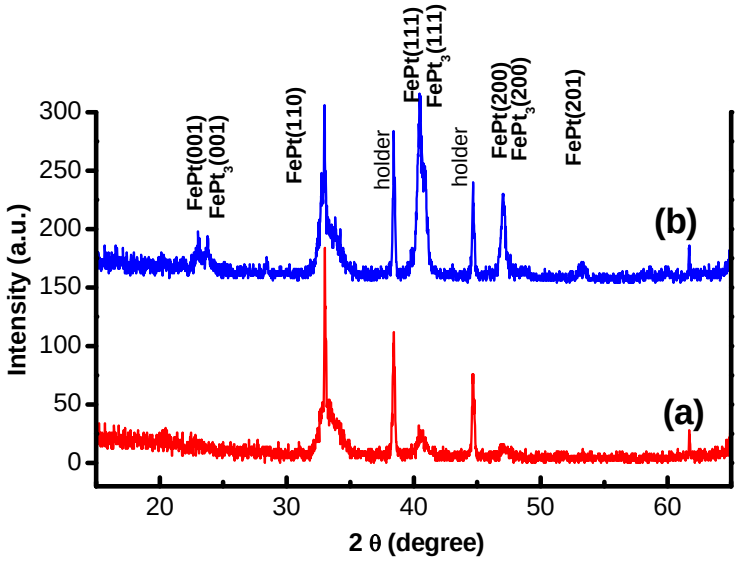

Figure 4.26 *XRD patterns of annealed FePt-$FePt_3$ with NaCl-to-FePt ratios of (a) 100:1, and (b) 40:1*

Chapter 5 Conclusions

1. The size control of FePt nanoparticles has been studied. By varying synthetic parameters including amount of the surfactants, the heating time and the heating temperature, the particle size from 3 to 8 nm can be obtained.
2. The composition of FePt nanoparticle depends on the size. With increasing particle size, there was an increase in Pt content.
3. The amount of the surfactants not only affects the size of FePt nanoparticles but also the composition.
4. Salt-matrix annealing can prevent FePt nanoparticles from sintering at high temperature. The size and shape can be retained. The coercivity of fct FePt nanoparticle is up to 10kOe.
5. The isolated nanocomposite of FePt-$FePt_3$ can be obtained by salt-matrix annealing. The new nanostructure presents exchange spring.

References

[1] U. Jeong, X. W. Teng, Y. Wang, H. Yang, Y. N. Xia, Advanced Materials 19 (2007) 33-60.
[2] N. Moumen, M. P. Pileni, Chemistry of Materials 8 (1996) 1128-1134.
[3] J. Frenkel, J. Dorfman, in: Nature(London), vol 126, 1930, p. 274.
[4] A. H. Lu, E. L. Salabas, F. Schuth, Angewandte Chemie-International Edition 46 (2007) 1222-1244.
[5] Y. Labaye, O. Crisan, L. Berger, J. M. Greneche, J. M. D. Coey, Surface anisotropy in ferromagnetic nanoparticles, in: 2002, pp. 8715-8717.
[6] F. Bodker, S. Morup, S. Linderoth, Physical Review Letters 72 (1994) 282-285.
[7] H. Zeng, J. Li, Z. L. Wang, J. P. Liu, S. H. Sun, Nano Letters 4 (2004) 187-190.
[8] Z. C. Xu, Y. L. Hou, S. H. Sun, Journal of the American Chemical Society 129 (2007) 8698-+.
[9] X. W. Teng, H. Yang, Synthesis of magnetic nanocomposites and alloys from platinum-iron oxide core-shell nanoparticles, in: 2005, pp. S554-S561.
[10] C. W. Lai, Y. H. Wang, B. P. Uttam, Y. C. Chen, J. K. Hsiao, C. L. Liu, H. M. Liu, C. Y. Chen, P. T. Chou, Chemical Communications (2008) 5342-5344.
[11] V. Nandwana, G. S. Chaubey, K. Yano, C. B. Rong, J. P. Liu, Journal of Applied Physics 105 (2009).
[12] J. Nogues, J. Sort, V. Langlais, V. Skumryev, S. Surinach, J. S. Munoz, M. D. Baro, Physics Reports-Review Section of Physics Letters 422 (2005) 65-117.
[13] W. L. Shi, H. Zeng, Y. Sahoo, T. Y. Ohulchanskyy, Y. Ding, Z. L. Wang, M. Swihart, P. N. Prasad, Nano Letters 6 (2006) 875-881.
[14] L. C. Varanda, M. Imaizumi, F. J. Santos, M. Jafelicci, Iron Oxide Versus Fe55Pt45/Fe3O4: Improved Magnetic Properties of Core/Shell Nanoparticles for Biomedical Applications, in: 2008, pp. 4448-4451.
[15] L. C. Varanda, M. Jafelicci, Journal of the American Chemical Society 128 (2006) 11062-11066.
[16] S. H. Sun, S. Anders, T. Thomson, J. E. E. Baglin, M. F. Toney, H. F. Hamann, C. B. Murray, B. D. Terris, Journal of Physical Chemistry B 107 (2003) 5419-5425.
[17] S. H. Sun, Advanced Materials 18 (2006) 393-403.
[18] S. H. Sun, C. B. Murray, D. Weller, L. Folks, A. Moser, Science 287 (2000) 1989-1992.
[19] N. Shukla, C. Liu, A. G. Roy, Materials Letters 60 (2006) 995-998.

[20] Y. L. Hou, H. Kondoh, R. C. Che, M. Takeguchi, T. Ohta, Small 2 (2006) 235-238.
[21] C. Wang, Y. L. Hou, J. M. Kim, S. H. Sun, Angewandte Chemie-International Edition 46 (2007) 6333-6335.
[22] V. Nandwana, K. E. Elkins, N. Poudyal, G. S. Chaubey, K. Yano, J. P. Liu, Journal of Physical Chemistry C 111 (2007) 4185-4189.
[23] N. Shukla, E. B. Svedberg, J. Ell, Colloids and Surfaces a-Physicochemical and Engineering Aspects 301 (2007) 113-116.
[24] M. Chen, J. P. Liu, S. H. Sun, Journal of the American Chemical Society 126 (2004) 8394-8395.
[25] M. Chen, J. Kim, J. P. Liu, H. Y. Fan, S. H. Sun, Journal of the American Chemical Society 128 (2006) 7132-7133.
[26] N. Shukla, M. M. Nigra, T. Nuhfer, M. A. Bartel, A. J. Gellman, Nanotechnology 20 (2009).
[27] B. Jeyadevan, K. Urakawa, A. Hobo, N. Chinnasamy, K. Shinoda, K. Tohji, D. D. J. Djayaprawira, M. Tsunoda, M. Takahashi, Japanese Journal of Applied Physics Part 2-Letters 42 (2003) L350-L352.
[28] Y. Ding, S. A. Majetich, J. Kim, K. Barmak, H. Rollins, P. Sides, Journal of Magnetism and Magnetic Materials 284 (2004) 336-341.
[29] M. Mizuno, Y. Sasaki, A. C. C. Yu, M. Inoue, Langmuir 20 (2004) 11305-11307.
[30] J. Sort, S. Surinach, M. D. Baro, D. Muraviev, G. I. Dzhardimalieva, N. D. Golubeva, S. I. Pomogailo, A. D. Pomogailo, W. A. A. Macedo, D. Weller, V. Skumryev, J. Nogues, Advanced Materials 18 (2006) 466-+.
[31] S. Yamamoto, Y. Morimoto, T. Ono, M. Takano, Applied Physics Letters 87 (2005).
[32] J. Kim, C. B. Rong, Y. Lee, J. P. Liu, S. H. Sun, Chemistry of Materials 20 (2008) 7242-7245.
[33] k. Elkins, D. Li, N. Poudyal, V. Nandwana, Z. Jim, K. Chen, J. P. Liu, Journal of Physics D: Applied Physics 38 (2005) 2306.
[34] C. L. Platt, K. W. Wierman, E. B. Svedberg, R. van de Veerdonk, J. K. Howard, A. G. Roy, D. E. Laughlin, Journal of Applied Physics 92 (2002) 6104-6109.
[35] K. Yano, V. Nandwana, N. Poudyal, C. B. Rong, J. P. Liu, Journal of Applied Physics 104 (2008).
[36] S. Saita, S. Maenosono, Journal of Physics-Condensed Matter 16 (2004) 6385-6394.
[37] J. R. Liu, K. Elkins, D. Li, V. Nandwana, N. Poudyal, Phase transformation of FePt nanoparticles, in: 2006, pp. 3036-3041.
[38] Y. W. Jun, J. H. Lee, J. Cheon, Angewandte Chemie-International Edition 47 (2008) 5122-5135.
[39] V. E. J. W., Nature(London) 144 (1939) 327.

[40] R. Aragon, Physical Review B 46 (1992) 5328-5333.
[41] V. V. Gridin, G. R. Hearne, J. M. Honig, Physical Review B 53 (1996) 15518-15521.
[42] G. Q. Gong, A. Gupta, G. Xiao, W. Qian, V. P. Dravid, Physical Review B 56 (1997) 5096-5099.
[43] J. M. D. Coey, A. E. Berkowitz, L. Balcells, F. F. Putris, F. T. Parker, Applied Physics Letters 72 (1998) 734-736.
[44] T. Fried, G. Shemer, G. Markovich, Advanced Materials 13 (2001) 1158-+.
[45] R. Vijayakumar, Y. Koltypin, I. Felner, A. Gedanken, Sonochemical synthesis and characterization of pure nanometer-sized Fe3O4 particles, in: 2000, pp. 101-105.
[46] S. H. Sun, H. Zeng, Journal of the American Chemical Society 124 (2002) 8204-8205.
[47] K. R. Brown, M. J. Natan, Langmuir 14 (1998) 726-728.
[48] S. H. Sun, H. Zeng, D. B. Robinson, S. Raoux, P. M. Rice, S. X. Wang, G. X. Li, Journal of the American Chemical Society 126 (2004) 273-279.
[49] H. Zeng, P. M. Rice, S. X. Wang, S. H. Sun, Journal of the American Chemical Society 126 (2004) 11458-11459.
[50] M. V. Kovalenko, M. I. Bodnarchuk, R. T. Lechner, G. Hesser, F. Schaffler, W. Heiss, Journal of the American Chemical Society 129 (2007) 6352-+.
[51] H. T. Yang, T. Ogawa, D. Hasegawa, M. Takahashi, Synthesis and magnetic properties of monodisperse magnetite nanocubes, in: 2008.
[52] D. Kim, N. Lee, M. Park, B. H. Kim, K. An, T. Hyeon, journal of the American Chemical Society 131 (2009) 454.
[53] M. Nakaya, M. Kanehara, T. Teranishi, Langmuir 22 (2006) 3485-3487.
[54] W. W. Yu, X. G. Peng, Angewandte Chemie-International Edition 41 (2002) 2368-2371.
[55] C. Srivastava, D. E. Nikles, G. B. Thompson, Journal of Applied Physics 104 (2008).
[56] K. Simeonidis, S. Mourdikoudis, I. Tsiaoussis, M. Angelakeris, C. Dendrinou-Samara, O. Kalogirou, Journal of Magnetism and Magnetic Materials 320 (2008) 1631-1638.
[57] H. G. Bagaria, D. T. Johnson, C. Srivastava, G. B. Thompson, M. Shamsuzzoha, D. E. Nikles, Journal of Applied Physics 101 (2007).
[58] T. B. Massalski, (1990).
[59] S. Ostanin, S. S. A. Razee, J. B. Staunton, B. Ginatempo, E. Bruno, Journal of Applied Physics 93 (2003) 453-457.
[60] S. Maat, O. Hellwig, G. Zeltzer, E. E. Fullerton, G. J. Mankey, M. L. Crow, J. L. Robertson, Physical Review B 63 (2001).
[61] H. Zeng, S. H. Sun, R. L. Sandstrom, C. B. Murray, Chemical ordering of FePt nanoparticle self-assemblies by rapid thermal annealing, in: 2003, pp. 227-232.

[62] H. Zeng, J. Li, J. P. Liu, Z. L. Wang, S. H. Sun, Nature 420 (2002) 395-398.
[63] C. H. Ho, C. H. Lai, Size-dependent magnetic properties of PtMn nanoparticles, in: 2006, pp. 3069-3071.